Excitation and correlation dynamics of a Rydberg quantum simulator using Numerical methods

A Thesis

submitted to

Indian Institute of Science Education and Research Pune

in partial fulfillment of the requirements for the

BS-MS Dual Degree Programme

by

Varna Shenoy K

Indian Institute of Science Education and Research Pune

Dr. Homi Bhabha Road,

Pashan, Pune 411008, INDIA.

April, **2023**

Supervisor: **Prof. Rejish Nath**

Certificate

This is to certify that this dissertation entitled Excitation and correlation dynamics of a Rydberg quantum simulator using Numerical methods towards the partial fulfilment of the BS-MS dual degree programme at the Indian Institute of Science Education and Research, Pune represents study/work carried out by **Varna Shenoy K** at Indian Institute of Science Education and Research under the supervision of **Prof. Rejish Nath** , **Associate Professor** , **Department of Physics** , during the academic year **2022-2023**.

Prof. Rejish Nath

Committee:

Prof. Rejish Nath

Prof. T S Mahesh

This thesis is dedicated to my parents, Poornima and Vishwanath and my grandmother Suguna.

Declaration

I hereby declare that the matter embodied in the report entitled Excitation and correlation dynamics of a Rydberg quantum simulator using Numerical methods are the results of the work carried out by me at the **Department of Physics** , Indian Institute of Science Education and Research, Pune, under the supervision of **Prof. Rejish Nath** and the same has not been submitted elsewhere for any other degree.

Varna Shenoy K

Acknowledgments

I am extremely grateful to my supervisor, Prof. Rejish Nath, for his guidance, constant support and patience. I am thankful to him for the skills that I have developed to become the researcher that I have grown into today. I am also very thankful to Prof. Weibin Li for being a collaborator on our project.

I am also extremely grateful to Prof. T S Mahesh, for being my thesis expert and for evaluating my thesis.

I am indebted to the director of IISER Pune, the institute and the National Supercomputing Mission for providing me with the opportunity to use PARAM Brahma, without which this project may not have been possible.

I am also very grateful to Vighnesh Naik, who started this project and who has helped me every step of the way and with whom I have had interesting discussions on academic topics from which I have learnt a lot.

I am very grateful to the PhD students and post-docs of our group, Dhiya, Sandra, Ratheejit, Siddharth and Inderpreet, for always being ready to help when I needed it, and for the enjoyable discussions and guidance.

Most importantly, I am indebted to my parents and grandparents for always supporting me, believing in me and encouraging me to pursue my dreams.

Abstract

This master's thesis investigates the excitation and correlation dynamics of a one-dimensional chain of Rydberg atoms with van der Waals interactions, utilizing two numerical methods: discrete truncated Wigner approximation (dTWA) and artificial neural networks (ANN). Specifically, the total number of excitations, the long-time average number of excitations, the maximum number of excitations, and second-order half-chain Rényi entanglement entropy is analyzed over time.

The research findings show that, for intermediate timescales and smaller interaction strengths, the 1st-order dTWA is effective in capturing the excitation dynamics. However, due to the numerical instability of the 2nd-order dTWA equations, this thesis proposes an approach to handle the instabilities by identifying and eliminating the terms causing the divergence in the 2-point correlation equations of motion. This method has resulted in delayed divergence and improved results compared to the 1st-order dTWA.

Additionally, this thesis demonstrates that the ANN approach provides a reliable method to capture the excitation dynamics and 2nd-order Renyi entanglement entropy, achieving better results with an increase in the number of parameters.

This thesis suggests further exploration of other neural network architectures for studying this system and the inclusion of higher-order dTWA to address the instability issue in the 2-point correlation equation of motion. Overall, these numerical methods could facilitate the development of theoretical and numerical tools for benchmarking and improving the performance of Rydberg quantum simulators. Therefore, this master's thesis highlights the potential of dTWA and ANN as powerful numerical methods for studying Rydberg quantum simulators.

List of Figures

Contents

Chapter 1

Introduction

Quantum many-body physics studies the properties and phenomena that take place in ensembles of interacting particles. With intersections with not only condensed matter but also nuclear and high-energy physics, this is a broad area of physics with much potential for applications. Despite decades of research, there are still many experimental phenomena in quantum many-body physics that lack a satisfactory theoretical explanation. One of the biggest challenges in this field is the *curse of dimensionality*, as the size of the Hilbert space grows exponentially with an increase in the number of particles, making it difficult to derive macroscopic properties from microscopic laws.

Exact methods can only handle systems with a small number of particles, and *classical computers* are unable to exactly compute the dynamics of large quantum many-body systems. To overcome this issue, researchers have developed various approximate numerical methods. However, the complexity of quantum many-body systems increases dramatically with the number of particles, making efficient simulation a daunting task. Entanglement is one of the many approaches used to describe the complexity of quantum many-body systems [1]. However, despite being a well-known concept, its precise role in hindering the efficient classical simulation of many-body systems is still being investigated. Various quantifications of entanglement have been developed to

measure this quantum resource, but a complete understanding of its impact on classical simulations is yet to be achieved.

One approach to studying quantum many-body systems suggested by Feynman involved building a computer based on quantum mechanics, or essentially constructing a synthetic quantum system on which models can be implemented and solved, which could not be done in other ways [2]. These synthetic quantum systems are quantum simulators. In a quantum simulator, there is a high degree of control over the particles and highly tunable interactions [3]. As quantum simulators using Rydberg atoms [4–11], trapped ions [12–14], polar molecules [15] and magnetic atoms [16,17] have become increasingly important in the study of complex quantum systems, the need for accurate numerical methods to analyze the behaviour of large-scale systems has become crucial. These numerical methods are necessary to ensure that the quantum simulators are performing as intended and accurately simulating the target system. Without such methods, it would be difficult to validate the results obtained from the simulators and gain insights into the properties of the target systems.

Many common approximation methods are based on tensor-network states, the most common of which is the time-dependent density matrix renormalisation group (t-DMRG), which is based on expressing the quantum states in terms of matrix product states [18–23]. This is based on the observation that the entire Hilbert space is not required to simulate the dynamics, and the Hilbert space can essentially be reduced now. The challenge is to find those relevant states that have a significant probability. DMRG involves truncating the density matrix at a certain order, known as the bond dimension. By increasing the bond dimension, the accuracy of the results can be improved, with convergence being reached at a certain bond dimension [24]. However, DMRG is limited to one-dimensional systems, and as the degree of entanglement in a system increases, the bond dimension required to achieve convergence grows exponentially with the size of the system. This makes it challenging to apply DMRG to larger systems with high degrees of entanglement.

This has led to the development of phase-space-based methods like discrete truncated Wigner approximation, where classical equations of motion are applied to initial states that are sampled from a phase space [25]. dTWA [26–30] has shown promising and well-matching results while

being used to simulate various systems [31–34]. Phenomena such as many-body localisation and thermalisation have also been studied using dTWA [35]. Another method being studied recently are the methods based on machine learning [36] where the wave function is considered approximately using a parameterisation, and these parameters are suitably chosen to efficiently represent the wave function. An Artificial neural network is used to efficiently represent the wave function, and reinforcement learning is then used to learn the parameters and get the dynamics of the system. ANNs have previously been used to efficiently get not only the ground state but also the dynamics of spin systems [37–43].

This thesis aims to investigate the applicability and limitations of two numerical methods, dTWA and ANN, in studying the excitation dynamics as well as entanglement in a chain of Rydberg atoms. Chapter (2) provides an introduction to Rydberg systems. Chapter (3) explains the dTWA method, while chapter (3.2) focuses on using neural networks to simulate quantum many-body systems. Chapter (4) presents and discusses the obtained results, and chapter (5) concludes the thesis.

Chapter 2

Rydberg Quantum simulator

A quantum simulator is a device that is designed to mimic and study the behaviour of quantum systems that are too complex to be simulated on classical computers. Quantum simulators are often based on physical systems that can be controlled and manipulated in a precise and controlled manner, such as atoms, ions, or superconducting circuits [5].

With experimental developments in the manipulation of individual quantum entities like atoms, molecules, ions etc, and advancements in cooling of atoms to the ultra-cold regime to nano-Kelvin temperatures [5], programmable quantum simulation with tunable parameters of a Hamiltonian has become a reality. In particular, the trapping of atoms in optical lattices [44–48] has led to individually controllable neutral ultracold atoms in traps at a distance of several micrometres. This development, combined with the power of tunable lasers capable of strongly coupling the ground state and the Rydberg state, has led to the development of Rydberg quantum simulators.

The Rydberg state [49] is a state with a really high principle quantum number n. This high n leads to a much longer lifetime ($\propto n^3$) than the low-lying states, which proves very advantageous. Another advantage is the strong interactions which are long-range and can be up to orders of a few micrometres. This strong interaction leads to the process of Rydberg blockade mechanism [50,51], which has made possible, the implementation of quantum gates [52,53], since, the excitation of one

atom to the Rydberg state prohibits the excitation of any other atom within a radius and this leads to the conditional excitation of an atom given the state of another atom. The theoretical description of this system has led to a natural map to spin systems, and this makes Rydberg quantum simulators an ideal bed for studying many-body spin systems.

In recent years, there has been significant progress in simulating many-body physics using quantum simulators, which have led to several important experimental advancements in condensed matter physics and quantum chemistry. Non-trivial quantum systems with a complexity level at which it becomes difficult or impossible to calculate the spin dynamics have been simulated using quantum simulators. These include coherent spin models, many-body motional dynamics, and driven-dissipative systems. Given below are some phenomena which have been studied using Rydberg quantum simulators [54].

Many-body localization: In these experiments, researchers use Rydberg atoms to simulate the behaviour of strongly interacting quantum particles in disordered systems. The goal is to understand the phenomenon of many-body localization, where a quantum system fails to thermalize and retains a memory of its initial conditions. Several experiments have observed many-body localization in Rydberg atom-based systems, including studies of quasiperiodic potentials, disordered potentials, and random field Ising models [55].

Quantum magnetism: In these experiments, researchers use Rydberg atoms to simulate the behaviour of spin systems, such as the Ising model and the Heisenberg model. By studying the dynamics and correlations of these systems, researchers can gain insights into the behaviour of real materials and systems, such as spin glasses and superconductors. Some recent experiments have demonstrated the simulation of long-range magnetic interactions using Rydberg atoms [56, 57].

Quantum phase transitions: In these experiments, researchers have used Rydberg quantum simulators to study the quantum dynamics across a phase transition and observed the formation of Rydberg crystals and different quantum phases that happen due to the phenomena of Rydberg blockade by adiabatically varying the detuning. These experiments have been done on a 1D array

of 51 qubits as well as a 2D lattice of 256 qubits [6, 58, 59].

Quantum simulators are also theorised to be capable of simulating the behaviour of gauge fields, which are essential to understanding the behaviour of elementary particles in high-energy physics. With such high potential, benchmarking quantum simulators becomes a very crucial task. So, in this chapter, we will first look at the phenomenon of Rydberg blockade, then followed by a description of the Hamiltonian and finally, we see how it can easily be mapped to a spin system.

2.1 Rydberg blockade mechanism

The Rydberg blockade mechanism is a phenomenon where the simultaneous excitation of two atoms within a radius is forbidden due to the strong interactions between atoms that are excited to a Rydberg state. When we have 2 atoms separated by a distance R where the ground state $|g\rangle$ and a specific Rydberg state $|r\rangle$ of each atom are coherently coupled using a resonant laser field with a Rabi frequency Ω, the state $|rr\rangle$ is shifted in energy by C_6/R^6 due to the van der Waals interaction.

The Rydberg blockade radius is given by

$$R_b = \left(\frac{C_6}{\hbar\Omega}\right)^{1/6} \tag{2.1}$$

And when the blockade condition $R << R_b$ is satisfied, then the state $|rr\rangle$ is out of resonance and is forbidden. This leads to Rabi oscillations between the ground state $|gg\rangle$ and the entangled state $(|gr\rangle + |rg\rangle)/\sqrt{2}$, with a coupling $\sqrt{2\Omega}$.

When a group of N atoms is confined within a blockade volume, only one Rydberg excitation is allowed at most. This results in a collective Rabi oscillation with an increased frequency of $\sqrt{N\Omega}$ between the collective ground state, represented by $|gg..g\rangle$, and the entangled state, represented by $|ggg..r_i..g\rangle$, where a single Rydberg excitation is distributed among all the atoms. However, if the system exceeds the blockade radius, multiple Rydberg atoms can be excited, but their positions

will be heavily dependent on the blockade restriction. This can lead to interesting phenomena like dynamical crystallisation.

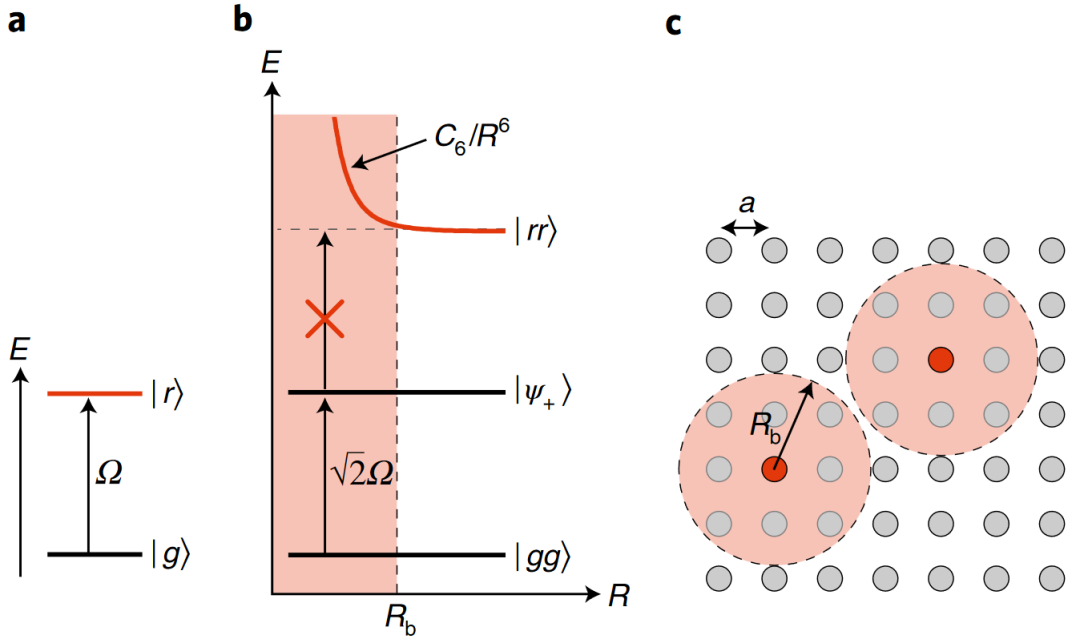

Figure 2.1: (a) shows the ground and Rydberg state of a single atom coupled by a laser Ω. (b) diagrammatically shows the Rydberg blockade mechanism and the out-of-resonance of the $|rr\rangle$ state due to the van der Waal interaction. (c) shows 2 Rydberg excitations and their blockade radius in a 2D array of atoms. This figure is taken from [5]

2.2 System description and mapping to spin systems

We consider N atoms as described in the previous section, each with a ground state $|g\rangle$ and a Rydberg state $|r\rangle$ coupled by a laser Ω and detuned by Δ. The interactions are van der Waal interactions, and they occur when two atoms are in the Rydberg state and are given by $V_{ij} = C_6/R_{ij}^6$. The Hamiltonian of such a system is given by [58],

$$\frac{\mathscr{H}}{\hbar} = \frac{\Omega}{2}\sum_i (|g_i\rangle\langle r_i| + |r_i\rangle\langle g_i|) - \Delta\sum_i n_i + \sum_{i<j} V_{ij} n_i n_j \tag{2.2}$$

We set the detuning $\Delta = 0$ and study the on-resonant case by initializing the system in a product state with all the atoms in the ground state [60]

$$|\Psi_0\rangle = \prod_i |g_i\rangle \tag{2.3}$$

A quantum quench is then performed with dynamics governed by the Hamiltonian $\mathscr{H}$ 2.2. The time evolution of state at time t is given by,

$$|\Psi(t)\rangle = e^{-\mathrm{i}\mathscr{H}t}\,|\Psi_0\rangle \tag{2.4}$$

To study the dynamics of our Hamiltonian, we map the Hamiltonian to that of a spin system. The states $|g\rangle$ and $|r\rangle$ are mapped to the eigenstates of the S_z operator, $|\downarrow\rangle$ and $|\uparrow\rangle$ respectively.

We do this by replacing n_i with $\frac{(1+\sigma_i^z)}{2}$.

$$\begin{aligned}\mathscr{H} &= \frac{\Omega}{2}\sum_i \sigma_i^x + \sum_{i<j}\frac{V_{ij}}{4}(1+\sigma_i^z+\sigma_j^z+\sigma_i^z\sigma_j^z)\\ &= \frac{\Omega}{2}\sum_i \sigma_i^x + \sum_i\sum_{j\neq i}\frac{V_{ij}}{4}\sigma_i^z + \sum_{i<j}\frac{V_{ij}}{4}\sigma_i^z\sigma_j^z - \frac{\Delta N}{2} + \sum_{i<j}\frac{V_{ij}}{4}\end{aligned} \tag{2.5}$$

On removing the constants, we are left with

$$\mathscr{H} = \frac{\Omega}{2}\sum_i \sigma_i^x + \sum_i\sum_{j\neq i}\frac{V_{ij}}{4}\sigma_i^z + \sum_{i<j}\frac{V_{ij}}{4}\sigma_i^z\sigma_j^z \tag{2.6}$$

We will now use this Hamiltonian and the numerical methods of discrete truncated Wigner approximation and artificial neural networks to study the excitation dynamics as well as entanglement growth in the system.

Chapter 3

Numerical Methods

In this chapter, we will describe the numerical methods used to simulate the dynamics of the quantum many-body Rydberg system. We will first describe the phase space methods of discrete truncated Wigner approximation followed by the machine learning approach of artificial neural networks

3.1 Discrete Truncated Wigner Approximation

The discrete truncated Wigner approximation (dTWA) is a semi-classical phase space method of studying quantum dynamics of many-body spin systems of arbitrary dimensions. It makes use of the Wigner-Weyl transform [61, 62] to map the dynamics in the Hilbert space to the dynamics in classical phase space [63]. dTWA goes a step further compared to the mean-field approximations since it incorporates the quantum uncertainty in the initial state by sampling from the Wigner function for the initial state [26]. Then each initial condition is evolved using classical equations of motion and averaged over the initial condition to get the expectation values of the observables. Here, the Bogoliubov-Born-Green-Kirkwood-Yvon (BBGKY) hierarchy is used to get the classical equations of motion [64]. The BBGKY hierarchy is used because it provides the advantage of

being able to include arbitrary n-point correlations in the equations of motion.

Motivation for considering phase-space representation of quantum mechanics

The Wigner function and Weyl transform provide an alternative framework for understanding quantum mechanics that is equivalent to the standard Schrödinger picture. In the conventional formulation of quantum mechanics, the wave function is used to represent the quantum state, and from it, one can obtain the probability distribution in the position and momentum basis. However, it is valuable to visualize the probability distribution in both position and momentum variables simultaneously. The Wigner function achieves this, but it is not a conventional probability distribution due to the inability to find a positive probability distribution everywhere, and it is therefore referred to as a quasi-probability distribution.

Consider the expectation value of an observable $\hat{O}$ in the standard representation of quantum mechanics. It is given by

$$\begin{aligned} \left\langle \hat{O} \right\rangle &= Tr[\hat{O}\rho] \\ &= \sum_{\nu} \sum_{\nu'} \langle \nu | \hat{O} | \nu' \rangle c_{\nu} c^*_{\nu'} \end{aligned} \tag{3.1}$$

Where the density matrix is given by the basis states $|\nu\rangle$ weighted by the coefficient c_{ν}. This form is similar to calculating the expectation value of an observable in statistical physics. This motivates us to consider a statistical description of quantum mechanics. Wigner, in 1932, aimed to find the quantum corrections to classical statistical mechanics where the Boltzmann factors contained energy expressed in terms of x and p and constructed the Wigner function as a quasi-probability distribution in both x and p. The Heisenberg uncertainty principle places constraints on the distribution, and the Wigner function cannot have any arbitrary value.

Since expectation values of observables have been a motivation for us to consider this alternate

formulation of quantum mechanics, we will see how we can reproduce the expectation values of physical observables using the Wigner function in the following section.

3.1.1 Continuous phase space representation

The expectation value of physical observables can be found using the Wigner function and the Weyl transform. The Weyl transform is critical to the phase-space representation of quantum mechanics, it maps any observable in the Hilbert space to a function in the classical phase-space.

Given an operator $\hat{\Omega}(\hat{x},\hat{p})$, the Weyl transform of this operator (denoted by subscript w) is given by

$$\Omega_{\mathrm{w}}(x,p) = \int dx' \left\langle x - \frac{x'}{2} \middle| \hat{\Omega}(\hat{x},\hat{p}) \middle| x + \frac{x'}{2} \right\rangle \exp\left(\frac{ipx'}{\hbar}\right) \tag{3.2}$$

The Wigner function is the Weyl transform of the density matrix and is given by

$$\mathscr{W}(x,p) = \int dx' \left\langle x - \frac{x'}{2} \middle| \hat{\rho} \middle| x + \frac{x'}{2} \right\rangle \exp\left(\frac{ipx'}{\hbar}\right) \tag{3.3}$$

One interesting property of the Weyl transform is that

$$\mathrm{Tr}[\hat{A}\hat{B}] = \frac{1}{h}\int\int A_{\mathrm{w}} B_{\mathrm{w}}\, dx\, dp \tag{3.4}$$

Using this property, if we calculate the expectation value of any observable, we have

$$\begin{aligned} \left\langle \hat{A} \right\rangle &= \mathrm{Tr}[\hat{\rho}\hat{A}] \\ &= \frac{1}{h}\int\int \mathscr{W}(x,p) A_{\mathrm{w}}\, dx\, dp \end{aligned} \tag{3.5}$$

We see that this has a form similar to the expectation value in statistical physics, and the Wigner function plays the role of the probability distribution function.

It is useful later while generalizing the phase space formalism to discrete phase space to invert equation 3.3 and write the density matrix in terms of the Wigner function as

$$\hat{\rho} = \int dx \int dp \; \mathscr{W}(x,p) \; \hat{\mathscr{A}}(x,p) \tag{3.6}$$

Here, $\hat{\mathscr{A}}(x,p)$ is known as the phase point operator. These are a set of hermitian operators which are defined for every point in the phase space.

We can also express the Wigner function in terms of the density matrix and the phase point operator as

$$\mathscr{W}(x,p) = \frac{1}{2\pi\hbar} \mathrm{Tr}\left(\hat{\rho}\hat{\mathscr{A}}(x,p)\right) \tag{3.7}$$

An important property of the phase point operator is that $\mathrm{Tr}\left[\hat{\mathscr{A}}(x,p)\right] = 1$, which will prove useful to us later. We now move on to describe quantum dynamics in the continuous phase space.

Quantum dynamics in continuous phase space

If we consider dynamics in a classical system, given a Hamiltonian $\mathscr{H}$, the dynamics of phase space points can be given by Hamilton's equations of motion

$$\frac{dx}{dt} = \{x, \mathscr{H}\}; \qquad \frac{dp}{dt} = \{p, \mathscr{H}\} \tag{3.8}$$

where $\{a,b\} = -a\Lambda b$ are the Poisson brackets and Λ is the symplectic operator.

These classical equations of motion determine a unique trajectory, along with the initial conditions. In cases where there is uncertainty in the initial condition, the observable of interest is averaged over the probability distribution of the initial conditions, denoted by $W_{cl}(x_0,p_0)$ and $A_{cl}(x,p,t)$ is the classical observable. The average is given by

$$\langle A_{cl}(x,p,t)\rangle = \int\int dx_0 \, dp_0 \, W_{cl}(x_0,p_0) A_{cl}(x(t),p(t),t) \tag{3.9}$$

However, in quantum mechanics, the uncertainty principle prevents us from exactly determining the position and momentum of a particle. We can instead use the Wigner function of the initial density matrix as the probability distribution in the quantum case. By considering this, we can write the equation

$$\left\langle \hat{A}(\hat{x},\hat{p}) \right\rangle \approx \int\int dx_0\, dp_0\, \mathscr{W}(x_0,p_0) A_{\mathrm{w}}(x(t),p(t),t) \tag{3.10}$$

to approximate the expectation value of the observable. Here, $A_{\mathrm{w}}(x(t),p(t),t)$ and $\mathscr{W}(x_0,p_0)$ represent the Wigner function and the quantum observable, respectively.

Let us see if this is a valid extrapolation to make from the classical to the quantum case. We know that the dynamics in the Hilbert space is given by the von Neumann equation,

$$\mathrm{i}\hbar \frac{\partial \hat{\rho}}{\partial t} = \left[\hat{\mathscr{H}}, \hat{\rho} \right] \tag{3.11}$$

To express this using Weyl symbols in the classical phase space, we need an expression for the commutator of two Weyl symbols $A_{\mathrm{w}}, B_{\mathrm{w}}$. This is given as,

$$\mathrm{C}_{\mathrm{A_w,B_w}} = \mathrm{i}\hbar \{A_{\mathrm{w}}, B_{\mathrm{w}}\}_{\mathrm{MB}} \tag{3.12}$$

The von Neumann equation in the phase space now becomes

$$\dot{\mathscr{W}} = \{\mathscr{H}_{\mathrm{W}}, \mathscr{W}\}_{\mathrm{MB}} \tag{3.13}$$

Here we use the Moyal bracket given by

$$\{a,b\}_{\mathrm{MB}} = -\frac{2}{\hbar} a \sin\left[\frac{\hbar}{2} \Lambda \right] b \tag{3.14}$$

Λ is the symplectic operator.

If $\hbar$ is small, we can expand sin in $\hbar$ to get

$$\sin\left[\frac{\hbar}{2}\Lambda\right] = \frac{\hbar}{2}\Lambda + \mathbf{O}(\hbar^3) \tag{3.15}$$

Then the Moyal bracket is

$$\{a,b\}_{\mathrm{MB}} = \{a,b\} + \mathbf{O}(\hbar^2) \tag{3.16}$$

We see that in the classical limit, the Moyal bracket reduces to the Poisson bracket, and the Wigner function reduces to the classical probability distribution, and our expression 3.10 is valid.

We have not considered higher powers of $\hbar$ in our above discussion, and this is where the truncation in the truncated Wigner approximation comes from, and the equations can be expanded to higher powers of $\hbar$ as well.

3.1.2 Discrete phase space representation

The formalism that we discussed in the previous section can only be applied for continuous degrees of freedom, and so W K Wootters generalised the Wigner function formalism to apply to systems having a finite number of orthogonal states in a discrete Hilbert space [65, 66]

In this thesis, we will, in particular, discuss the discrete phase space formalism for a system of spin $1/2$ particles. For a single spin $1/2$ particle, its quantum phase space can be represented by a real-valued finite field spanned by 4 points in a 2×2 phase space. Each point represents a state in phase space and is represented as a two-dimensional vector $\boldsymbol{\alpha} = (\alpha_1, \alpha_2)$ where $\alpha_1, \alpha_2 \in \{0,1\}$.

In this formulation, as in the continuous case, we define a phase point operator for each point in the phase space given by,

$$\begin{aligned} \hat{\mathscr{A}}_{\boldsymbol{\alpha}} &= \frac{1}{2}\left[\hat{I} + (-1)^{\alpha_2}\sigma_x + (-1)^{\alpha_1+\alpha_2}\sigma_y + (-1)^{\alpha_1}\sigma_z\right] \\ &= \frac{1}{2}\left[\hat{I} + \boldsymbol{r}_\alpha \cdot \boldsymbol{\sigma}\right] \end{aligned} \tag{3.17}$$

Where $\boldsymbol{\sigma} = (\sigma_x, \sigma_y, \sigma_z)$ and $\boldsymbol{r}_\alpha = ((-1)^{\alpha_2}, (-1)^{\alpha_1+\alpha_2}, (-1)^{\alpha_1})$

Analogous to eqn. 3.7, we then have the discrete Wigner function given by,

$$\mathscr{W}_\alpha = \frac{1}{2}\mathrm{Tr}\left[\hat{\rho}\hat{\mathscr{A}}_\alpha\right] \tag{3.18}$$

The Wigner function is the Weyl symbol of the density operator and generalising on eqn. 3.18, we can define the Weyl symbol of any observable $\hat{\Omega}$ as

$$\Omega_\mathrm{w} = \frac{1}{2}\mathrm{Tr}\left[\hat{\Omega}\hat{\mathscr{A}}_\alpha\right] \tag{3.19}$$

Up until now, we had discussed the phase space representation of a single spin $1/2$ particle represented by a 2×2 phase space. Now for a system of N spin half particles, their phase space can be represented as a tensor product of the phase space of the individual particles. For a product state, the phase point operator is given as

$$\hat{\mathscr{A}}_{\boldsymbol{\alpha}} = \hat{\mathscr{A}}_{\boldsymbol{\alpha}_1} \otimes \hat{\mathscr{A}}_{\boldsymbol{\alpha}_2} \otimes \hat{\mathscr{A}}_{\boldsymbol{\alpha}_3} \otimes ..... \otimes \hat{\mathscr{A}}_{\boldsymbol{\alpha}_N} \tag{3.20}$$

where $\boldsymbol{\alpha} = (\boldsymbol{\alpha}_1, \boldsymbol{\alpha}_2, \boldsymbol{\alpha}_3, ..., \boldsymbol{\alpha}_N)$ and $\boldsymbol{\alpha}_i$ is the 2×2 phase space of the ith particle. Analogous to eqn. 3.6, we can write the density matrix as a linear combination of the Wigner function and the phase point operator,

$$\hat{\rho} = \sum_\alpha \mathscr{W}_{\boldsymbol{\alpha}} \hat{\mathscr{A}}_{\boldsymbol{\alpha}} \tag{3.21}$$

The expectation value of any observable can be taken using the density matrix in this form as

$$\begin{aligned} \left\langle \hat{A} \right\rangle &= \mathrm{Tr}[\hat{A}\hat{\rho}] \\ &= \sum_{\boldsymbol{\alpha}} \mathscr{W}_{\boldsymbol{\alpha}} \mathrm{Tr}\left[\hat{A}\hat{\mathscr{A}}_{\boldsymbol{\alpha}}\right] \\ &= \sum_{\boldsymbol{\alpha}} \mathscr{W}_{\boldsymbol{\alpha}} A_{\boldsymbol{\alpha}} \end{aligned} \tag{3.22}$$

This expression is similar to eqn. 3.5 in the continuous case with the Wigner function as the PDF.

Quantum Dynamics in the discrete phase space

In the case of the continuous phase space, we looked at the time evolution of the Wigner function and got the time evolution of the system. But, another approach would be to evolve the density matrix by keeping the Wigner function constant and evolving the phase point operator from eqn. 3.21 in the Schrodinger picture using the time evolution operator. This approach will prove useful to us since we will see that we can include arbitrary n-point correlations in this method.

If $\hat{\rho}_0$ is our density matrix at our initial condition, we have

$$\hat{\rho}_0 = \sum_{\boldsymbol{\alpha}} \mathscr{W}_{\boldsymbol{\alpha}} \hat{\mathscr{A}}_{\boldsymbol{\alpha}} \tag{3.23}$$

For a product state, we can write the Wigner function as the product of the Wigner functions of the individual particles. Now, using eqn. 3.20, we have

$$\hat{\rho}_0 = \sum_{\boldsymbol{\alpha}} \prod_{i=1}^{N} \mathscr{W}_{\boldsymbol{\alpha}_i} \hat{\mathscr{A}}_{\boldsymbol{\alpha}_1} \otimes \hat{\mathscr{A}}_{\boldsymbol{\alpha}_2} \otimes ..... \otimes \hat{\mathscr{A}}_{\boldsymbol{\alpha}_N} \tag{3.24}$$

We can then write the density matrix at time t as

$$\hat{\rho}(t) = \sum_{\boldsymbol{\alpha}} \prod_{i=1}^{N} \mathscr{W}_{\boldsymbol{\alpha}_i} \hat{\mathscr{A}}^{\alpha_1 \ldots \alpha_N}_{1 \ldots N}(t) \tag{3.25}$$

Here, $\hat{\mathscr{A}}^{\alpha_1 \ldots \alpha_N}_{1 \ldots N}(t)$ is the time-dependent phase point operator given by applying unitary time-evolution operators

$$\hat{\mathscr{A}}^{\alpha_1 \ldots \alpha_N}_{1 \ldots N}(t) = U(t)\ \hat{\mathscr{A}}_{\alpha_1} \otimes \hat{\mathscr{A}}_{\alpha_2} \otimes ..... \otimes \hat{\mathscr{A}}_{\alpha_N}\ U^{\dagger}(t) \tag{3.26}$$

Where, $U(t) = \exp(-\mathrm{i}\mathscr{H}t)$ is the time evolution operator with a general Hamiltonian with on-site interaction $\mathscr{H}_i$ and pair-wise interaction term $\mathscr{H}_{ij}$

$$\mathscr{H} = \sum_i \mathscr{H}_i + \sum_{i<j} \mathscr{H}_{ij} \tag{3.27}$$

The equations of motion for the phase point operators $\hat{\mathscr{A}}_{1\ldots N}^{\alpha_1\ldots\alpha_N}(t)$ are given by the von Neumann equation

$$i\frac{\partial}{\partial t}\hat{\mathscr{A}}_{1\ldots N}^{\alpha_1\ldots\alpha_N}(t) = \left[\mathscr{H}, \hat{\mathscr{A}}_{1\ldots N}^{\alpha_1\ldots\alpha_N}\right] \tag{3.28}$$

This differential equation cannot be solved exactly, so we make use of reduced phase point operators like the reduced density matrix. Since the trace of the phase point operator is 1, it acts like a quasi-density matrix even though it is not positive definite.

$$\hat{\mathscr{A}}_i^{\alpha_1\ldots\alpha_N} = \mathrm{Tr}_{\not i}\hat{\mathscr{A}}_{1\ldots N}^{\alpha_1\ldots\alpha_N}, \qquad \hat{\mathscr{A}}_{ij}^{\alpha_1\ldots\alpha_N} = \mathrm{Tr}_{\not i\not j}\hat{\mathscr{A}}_{1\ldots N}^{\alpha_1\ldots\alpha_N} \tag{3.29}$$

where $\mathrm{Tr}_{\not i}$ denotes a partial trace over all the indices except i.

Using these reduced phase point operators, we can get the equations of motion by writing the BBGKY hierarchy of equations for the reduced phase point operators just like how they are written for the reduced density matrices.

We write the BBGKY hierarchy of equations in terms of the correlations $\mathscr{C}_{ij}$ using the cluster expansion [67] for the phase point operator $\hat{\mathscr{A}}_{1\ldots N}^{\alpha_1\ldots\alpha_N}$ given by

$$\begin{aligned}
\hat{\mathscr{A}}_{ij} &= \hat{\mathscr{A}}_i\hat{\mathscr{A}}_j + \hat{\mathscr{C}}_{ij} \\
\hat{\mathscr{A}}_{ijk} &= \hat{\mathscr{A}}_i\hat{\mathscr{A}}_j\hat{\mathscr{A}}_k + \hat{\mathscr{C}}_{jk}\hat{\mathscr{A}}_i + \hat{\mathscr{C}}_{ik}\hat{\mathscr{A}}_j + \ldots. + \hat{\mathscr{C}}_{ijk}
\end{aligned} \tag{3.30}$$

and similarly for higher orders.

Here we have dropped the superscript $\alpha_1\ldots\alpha_N$ and the terms $\hat{\mathscr{A}}_1, \hat{\mathscr{A}}_2, \ldots, \hat{\mathscr{A}}_N$ correspond to the uncorrelated parts of $\hat{\mathscr{A}}_{1\ldots N}^{\alpha_1\ldots\alpha_N}$, and the terms $\hat{\mathscr{C}}_{ij}, \hat{\mathscr{C}}_{ijk}\ldots$ correspond to the correlations that arise due interactions.

The first two equations of the BBGKY hierarchy in terms of these operators as:

$$
\begin{aligned}
\mathrm{i}\frac{\partial}{\partial t}\hat{\mathscr{A}_i} &= [\mathscr{H}_i, \hat{\mathscr{A}_i}] + \sum_{k\neq i} \mathrm{Tr}[\mathscr{H}_{ik}, \hat{\mathscr{C}_{ik}} + \hat{\mathscr{A}_i}\hat{\mathscr{A}_k}] \\
i\frac{\partial}{\partial t}\hat{\mathscr{C}_{ij}} &= [\mathscr{H}_i + \mathscr{H}_j + \mathscr{H}^{\mathrm{H}}_{i\not j} + \mathscr{H}^{\mathrm{H}}_{j\not i}, \hat{\mathscr{C}_{ij}}] + [\mathscr{H}_{ij}, \hat{\mathscr{C}_{ij}} + \hat{\mathscr{A}_i}\hat{\mathscr{A}_j}] + \sum_{k\neq i,j} (\mathrm{Tr}_k[\mathscr{H}_{ik}, \hat{\mathscr{A}_i}\hat{\mathscr{C}_{jk}}] + \mathrm{Tr}_k[\mathscr{H}_{jk}, \hat{\mathscr{A}_j}\hat{\mathscr{C}_{jk}}]) \\
&\quad - \hat{\mathscr{A}_i}\mathrm{Tr}_i[\mathscr{H}_{ij}, \hat{\mathscr{C}_{ij}} + \hat{\mathscr{A}_i}\hat{\mathscr{A}_j}] - \hat{\mathscr{A}_j}\mathrm{Tr}_j[\mathscr{H}_{ij}, \hat{\mathscr{C}_{ij}} + \hat{\mathscr{A}_i}\hat{\mathscr{A}_j}] + \sum_{k\neq i,j} (\mathrm{Tr}_k[\mathscr{H}_{ik}, \hat{\mathscr{C}_{ijk}}] + \mathrm{Tr}_k[\mathscr{H}_{jk}, \hat{\mathscr{C}_{ijk}}])
\end{aligned}
\tag{3.31}
$$

where $\mathscr{H}^{\mathrm{H}}_{i\not j}$ is a Hartree operator or Mean-field operator given by:

$$
\mathscr{H}^{\mathrm{H}}_{i\not j} = \sum_{k\neq i,j} \mathrm{Tr}_k(\mathscr{H}_{ik}\hat{A}_k) \tag{3.32}
$$

We can write similar equations for higher orders as well.

If we ignore all the correlations, we are left with only the first equation in eqn. 3.31 and we have the 1st order dTWA equation, if we consider only 2 point correlations and ignore the higher order equations, we have the 2nd order dTWA, and in this thesis, we have only considered the 1st order and 2nd order dTWA.

For a spin system, we can write the reduced phase point operator and 2-point correlation in the Pauli basis as

$$
\hat{\mathscr{A}_i} = \frac{1}{2}(I + a_i \cdot \boldsymbol{\sigma}) \tag{3.33}
$$

$$
\hat{\mathscr{C}_{ij}} = \frac{1}{4} \sum_{\mu,\nu\in\{x,y,z\}} c^{\mu\nu}_{ij}\, \sigma^{\mu}_i \sigma^{\nu}_j \tag{3.34}
$$

Using these equations in the BBGKY hierarchy equations of motion 3.31 for the time evolution of our Hamiltonian 2.6 from 2 gives us,

$$\frac{1}{2}\dot{a}_i^\mu = \sum_\delta \left[\frac{\Omega}{2} a_i^\delta \in^{\mu x\delta} + \sum_i \sum_{j\neq i} \frac{V_{ij}}{4} a_i^\delta \in^{\mu z\delta} + \left(G_i^z a_i^\delta + G_i^{z\delta} \right) \in^{\mu z\delta} \right] \tag{3.35}$$

$$\begin{aligned}
\frac{1}{2}\dot{c}_{ij}^{\mu\nu} = & \sum_\beta \left[\left(\frac{V_{ij}}{4} a_i^\beta \ \delta_{\nu,z} - \frac{V_{ij}}{4} a_j^\beta \ \delta_{\mu,z} \right) \in^{\mu\nu\beta} \right] + \sum_\delta \left[\frac{\Omega}{2} c_{ij}^{\delta\nu} \in^{x\delta\mu} + \left(\sum_i \sum_{j\neq i} \frac{V_{ij}}{4} c_{ij}^{\delta\nu} + G_{i/}^z \, c_{ij}^{\delta\nu} \right) \in^{z\delta\mu} \right] \\
& + \sum_\delta \left[\frac{\Omega}{2} c_{ij}^{\mu\delta} \in^{x\delta\nu} + \left(\sum_i \sum_{j\neq i} \frac{V_{ij}}{4} c_{ij}^{\mu\delta} + G_{j/}^z \, c_{ij}^{\mu\delta} \right) \in^{z\delta\nu} \right] + \sum_\delta \left[G_{ij}^{\nu z} a_i^\delta \ \in^{z\delta\mu} + G_{ji}^{\mu z} a_j^\delta \ \in^{z\delta\nu} \right] \\
& - \sum_\delta \frac{V_{ij}}{4} \left[a_i^\mu \left(c_{ij}^{z\delta} + a_i^z a_j^\delta \right) \in^{z\delta\nu} + a_j^\nu \left(c_{ij}^{\delta z} + a_i^\delta a_j^z \right) \in^{z\delta\mu} \right]
\end{aligned} \tag{3.36}$$

where

$$\begin{aligned}
G_i^z &= \sum_{k\neq i} \frac{V_{ik}}{4} a_k^z \,, & G_i^{z\delta} &= \sum_{k\neq i} \frac{V_{ik}}{4} c_{ki}^{z\delta} \\
G_{i/}^z &= \sum_{k\neq i,j} \frac{V_{ik}}{4} a_k^z \,, & G_{ij}^{\nu z} &= \sum_{k\neq i,j} \frac{V_{ik}}{4} c_{jk}^{\nu z}
\end{aligned}$$

We calculate the time evolution of the phase point operator by evolving the above equations, and we get the initial conditions of a_i^μ and $c_{ij}^{\mu\nu}$

$$a_i^\mu = \mathrm{Tr}\left(\sigma_i^\mu \hat{\mathscr{A}}_{1\ldots N}^{\alpha_1\ldots\alpha_N}(0) \right) \tag{3.37}$$

$$c_{ij}^{\mu\nu} = \mathrm{Tr}\left(\sigma_i^\mu \sigma_j^\nu \hat{\mathscr{A}}_{1\ldots N}^{\alpha_1\ldots\alpha_N}(0) \right) - a_i^\mu a_j^\nu \tag{3.38}$$

We start with a product state and $c_{ij}^{\mu\nu} = 0$.

After calculating the phase point operator for every time t, we can calculate the expectation value of one spin and two spin functions by using

$$\left\langle \sigma_i^\mu \right\rangle(t) = \mathrm{Tr}\left(\sigma_i^\mu \hat{\rho}(t) \right) = \sum_\alpha W_\alpha \mathrm{Tr}\left(\sigma_i^\mu \hat{\mathscr{A}}_{1\ldots N}^{\alpha_1\ldots\alpha_N}(t) \right) = \sum_\alpha W_\alpha a_i^\mu(t) \tag{3.39}$$

Similarly,

$$\left\langle \sigma_i^\mu \sigma_j^\nu \right\rangle (t) = \mathrm{Tr}\left(\sigma_i^\mu \sigma_j^\nu \hat{\rho}(t)\right) = \sum_\alpha W_\alpha \mathrm{Tr}\left(\sigma_i^\mu \sigma_j^\nu \hat{\mathscr{A}}_{1\ldots N}^{\alpha_1 \ldots \alpha_N}(t)\right) = \sum_\alpha W_\alpha \left(c_{ij}^{\mu\nu}(t) + a_i^\mu(t) a_j^\nu(t)\right) \tag{3.40}$$

For a very large system size, we will use the Monte Carlo procedure instead of calculating these summations exactly. So We sample N_s phase-space points α from the probability distribution W_α. The expectation values then become,

$$\begin{aligned} \left\langle \sigma_i^\mu \right\rangle (t) &\approx \frac{1}{N_s} \sum_{\alpha \in S} a_i^\mu(t) \\ \left\langle \sigma_i^\mu \sigma_j^\nu \right\rangle (t) &\approx \frac{1}{N_s} \sum_{\alpha \in S} \left(c_{ij}^{\mu\nu}(t) + a_i^\mu(t) a_j^\nu(t)\right) \end{aligned} \tag{3.41}$$

where S is the sample-space, and N_s is the total number of elements in S.

Summary

1. Sample phase points α from the probability distribution $\prod_i^N \mathscr{W}_{\alpha_i} = \frac{1}{2^N} \mathrm{Tr}\left(\rho_0 \hat{\mathscr{A}}_{1\ldots N}^{\alpha_1 \alpha_2 \ldots \alpha_N}(0)\right)$ of the initial density matrix ρ_0

2. Calculate the initial conditions of a_i^μ and $c_{ij}^{\mu\nu}$ using eqn. 3.37.

3. Time evolve the coefficients of the reduced phase point operator and 2-point correlations using eqns. 3.35 and 3.36.

4. Calculate the expectation values of one-spin and two-spin functions using 3.41

3.2 Artificial Neural Networks

In quantum many-body physics, exact solutions to problems are often unattainable due to the exponential number of amplitudes that must be stored when solving the Schrodinger equation. This challenge becomes even more pronounced as the size of the system increases. As a result, simulating non-equilibrium time evolution numerically and efficiently is crucial. While well-established methods exist for systems with area law entanglement growth, such as tensor networks and density matrix renormalisation group, they may not be effective for simulating higher dimensional or strongly correlated systems. To address this issue, physicists are exploring machine learning techniques to efficiently simulate these complex systems by encoding the quantum many-body state in an artificial neural network (ANN) [36–38, 68].

3.2.1 Neural Quantum State

Consider a spin system of size L. One can then represent quantum many-body wave function $\Psi(S)$ for a spin configuration $S = (s_1, s_2, ..., s_L)$ as

$$|\Psi\rangle = \sum_S \Psi(S)\,|S\rangle \tag{3.42}$$

Instead of relying on a stored value for $\Psi(S)$, we adopt a strategy where we generate $\Psi(S)$ on the fly using a versatile variational wave function that is defined by parameters $\alpha = (\alpha_1, \alpha_2, ..., \alpha_M)$ with M much less than L. Consequently, we can approximate $\Psi(S)$ with $\Psi(\alpha, S)$. The expectation value of any Observable $\hat{A}$ is then given by

$$\langle \hat{A} \rangle = \sum_S |\Psi(\alpha, S)|^2 \, \frac{\langle S|\hat{A}|\Psi(\alpha)\rangle}{\langle S|\Psi(\alpha)\rangle} \tag{3.43}$$

Efficient computation of the expectation value can be achieved by utilizing Monte Carlo sampling, where the probability distribution is represented by $|\Psi(\alpha, S)|^2$. A significant advantage of

this method is the absence of a sign problem.

Artificial neural networks (ANNs) have the potential to serve as highly adaptable variation wave functions due to their ability to work as universal function approximators. This means that a properly-sized ANN can be utilized to represent any quantum many-body wave function, allowing for effective convergence testing of simulation results through manipulation of network size as a control parameter. Additionally, the use of the gradient backpropagation algorithm facilitates efficient numerical treatment of this class of variational wave functions. The Artificial Neural Networks (ANNs) utilized to represent quantum many-body systems can be referred to as Neural Quantum States.

Various types of artificial neural networks, such as Convolutional Neural Networks (CNNs) and Recurrent Neural Networks (RNNs), have been utilized in the study of quantum dynamics. However, for the purpose of this thesis, we will focus exclusively on the Restricted Boltzmann Machine (RBM). It is worth noting that ANNs encode the logarithm of the wave function amplitudes rather than the amplitudes themselves. This is because storing large wavefunction amplitudes in their original form can be computationally challenging, whereas the logarithm of these coefficients can be more easily represented. Additionally, utilizing the logarithm in the backpropagation algorithm can facilitate numerical stability and prevent issues with vanishing gradients, making training the ANN more effective.

Restricted Boltzmann Machine as neural quantum state

The Restricted Boltzmann Machine (RBM) is a type of neural network consisting of two layers, a visible layer and a hidden layer. The visible layer is comprised of neurons representing the spin configuration S in our case, while the hidden layer consists of hidden neurons.

To generate a quantum many-body wave function, the RBM takes the spin configuration S as input and applies a dense function to it, with the $logcosh$ activation function utilized to produce

the output. Specifically, this process involves computing the dot product of the visible and hidden layers' weights and biases, followed by the application of the activation function to generate the RBM's output.

The wave function of the quantum many-body system for a given spin configuration S can be represented using the RBM as $\Psi(S,\mathscr{W})$, where $\mathscr{W} = (\vec{b},\vec{W})$ represents the RBM's biases and weights. In particular, the logarithm of the wave function can be written as:

$$\log(\Psi(S,\mathscr{W})) = \sum_{j=1}^{M} \log\cosh\left(b_j + \sum_{i=1}^{L} W_{ij}s_i\right) \tag{3.44}$$

Here, M represents the number of hidden neurons in the RBM, and L represents the number of visible neurons, i.e., the spin configuration S. The biases b_j and weights W_{ij} are optimized through machine learning techniques in order to accurately represent the quantum many-body wave function. The RBM's ability to capture the correlations between the spins in the system is determined by the values of these biases and weights, making their optimization a critical aspect of using RBMs as neural quantum states.

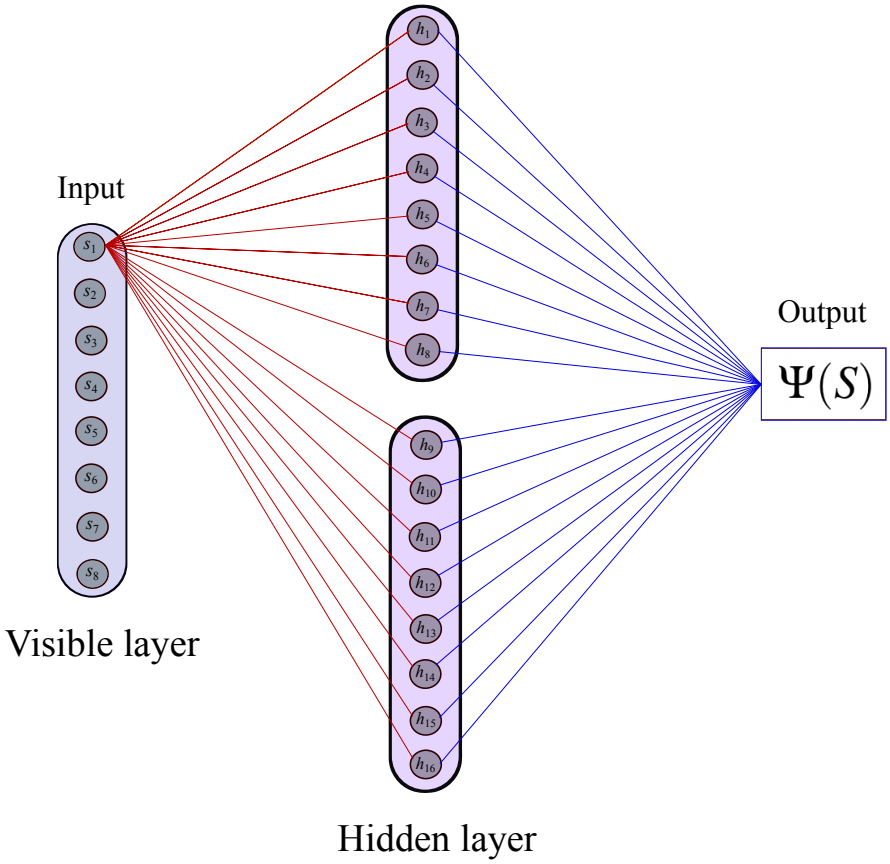

Figure 3.1: Schematic representation of an RBM with $N = 8$ visible units and $M = 16$ hidden units. Here every neuron in the visible layer is connected to every neuron in the hidden layer [60]

3.2.2 Training of neural quantum states

To train or optimize neural quantum states for dynamically changing quantum many-body states, we minimize the distance between time-evolved wave functions $e^{-iHdt}|\Psi(\alpha)\rangle$ and $|\Psi(\alpha+\dot{\alpha}dt)\rangle$ using the Fubini-Study metric. This metric captures the distance between two quantum states, taking into account their phases as well as magnitudes.

By minimizing the distance between the time-evolved wave functions, we can effectively learn the time-dependent parameters $\alpha(t)$ of the neural quantum state, which in turn can be used to

accurately represent the time-evolving quantum many-body states. This approach gives rise to a time-dependent variational principle (TDVP), which provides a powerful framework for studying dynamic quantum systems using neural networks.

3.2.3 Time-dependent Variational Principle

Consider the distance between $|\phi\rangle = e^{-iHdt}|\Psi(\alpha)\rangle$ and $|\psi\rangle = |\Psi(\alpha + \dot{\alpha}dt)\rangle$ in the Fubini-Study metric.

$$\mathscr{D}(|\psi\rangle,\ |\phi\rangle)^2 = \arccos\left(\sqrt{\frac{\langle\psi|\phi\rangle\langle\phi|\psi\rangle}{\langle\psi|\psi\rangle\langle\phi|\phi\rangle}}\right)^2 \tag{3.45}$$

We take dt very small, up to the first order, we can write

$$\langle S|\psi\rangle = \langle S|\left(1 - i\ dt\ H\right)|\Psi(\alpha)\rangle = \left(1 - i\ dt\ \mathrm{E}_{loc}(S)\right)\ \Psi(S,\alpha) \tag{3.46}$$

$$\langle S|\phi\rangle = \langle S|\Psi(\alpha)\rangle + \ dt\ \dot{\alpha}_k\ \frac{\partial}{\partial k}\langle S|\Psi(\alpha)\rangle = \left(1 + \ dt\ \dot{\alpha}_k \mathrm{O}_k(S)\right)\ \Psi(S,\alpha) \tag{3.47}$$

where E_{loc} is the local Energy given by $\mathrm{E}_{loc}(S) = \frac{\langle S|H|\Psi(\alpha)\rangle}{\langle S|\Psi(\alpha)\rangle}$ and O_k's are the gradients of the network given by $\mathrm{O}_k = \frac{\partial}{\partial k} log(\Psi(S,\alpha))$. Here we considered only up to the first order because second-order terms would cancel in the calculation.

Keeping only up to the second order in dt and using the expansion $\arccos\left(\sqrt{1+x}\right)^2 = x + \mathscr{O}(x^2)$, we finally get

$$\mathscr{D}(|\psi\rangle,\ |\phi\rangle)^2 = dt^2(\dot{\alpha}_k^*\ S_{kk'}\ \dot{\alpha}_k' - F_k^*\dot{\alpha}_k - F_k\dot{\alpha}_k^* + \mathrm{Var}(H)) \tag{3.48}$$

where $S_{kk'}$ is the covariance matrix and F_k is the generalised force vector and are defined as:

$$S_{kk'} = \langle \mathrm{O}_k \mathrm{O}_{k'}^* \rangle - \langle \mathrm{O}_k \rangle \langle \mathrm{O}_{k'}^* \rangle \tag{3.49}$$

$$F_k = -i\left(\langle \mathrm{E}_{loc} \mathrm{O}_k^* \rangle - \langle \mathrm{E}_{loc} \rangle \langle \mathrm{O}_k^* \rangle\right) \tag{3.50}$$

Minimizing $\mathscr{D}(|\psi\rangle, |\phi\rangle)^2$ with respect to $\dot{\alpha}_k$ gives the TDVP equation

$$S_{kk'}\dot{\alpha}_{k'} = F_k \tag{3.51}$$

To train the model, we compute $S^{-1}_{kk'}F_k$ using gradients O_k and the local energy E_{loc} using the Monte-Carlo sampling and solve the differential equation using the adaptive Heun scheme [38].

3.2.4 Summary

1. **Initialization of neural network parameters:**

   The network can be initialised with random weights chosen from a uniform distribution. Then a ground state search is done where the network parameters are trained to get the ground state of a Hamiltonian whose ground state is the required initial condition (H_{gs}). The network parameters are evolved to minimise the energy

   $$E(\alpha) = \sum_S |\Psi(S,\alpha)|^2 \frac{\langle S|H_{gs}|\Psi(\alpha)\rangle}{\langle S|\Psi(\alpha)\rangle}$$

   This is done until the variance of the energy is less than a cutoff and at this point, we get the network parameters which best represents the neural network. In certain cases, the neural network parameters for the initial state can also be found analytically.

2. **Sampling using Monte-Carlo:**

   Markov chain Monte Carlo is performed using the Metropolis-Hasting algorithm with a single spin flip in every step to sample from $|\Psi(S)|^2$.

3. **Measure the observables:**

   Now that $|\Psi(S)|^2$ has been sampled from, we calculate the expectation value of the observables $\hat{O}$ by using

   $$\langle\Psi(\alpha)|\hat{O}|\Psi(\alpha)\rangle = \sum_S |\Psi(S,\alpha)|^2 \frac{\langle S|\hat{O}|\Psi(\alpha)\rangle}{\langle S|\Psi(\alpha)\rangle} \tag{3.52}$$

4. **Update parameters using TDVP equation:**

   We update the parameters of the network using the TDVP equation

$$S_{kk'}\dot{\alpha}_{k'} = F_k \tag{3.53}$$

   The adaptive Heun scheme is used for solving the differential equation.

5. **Step 2 to step 4 is repeated until the maximum time is reached.**

Chapter 4

Results and Discussion

Now that we have discussed the numerical methods of dTWA and ANN, we will discuss the results obtained by applying these methods to a one-dimensional array of Rydberg atoms. We will compare the results obtained with those from exact diagonalisation and look at how well these methods work as well as their limitations. We will look at the excitation dynamics as well as the growth of entanglement entropy with time.

4.1 Results of the Excitation Dynamics

We study the dynamics of the total number of excitation N_e given by

$$N_e(t) = \sum_{i=1}^{N} \langle \Psi(t) | n_i | \Psi(t) \rangle \tag{4.1}$$

We also look at the maximum number of excitations during the time evolution of the system and also at the long time average of the total number of excitations

$$\overline{N}_e = \lim_{T \to \infty} \frac{1}{T} \int_0^T N_e(t) \tag{4.2}$$

4.1.1 Results from Exact Diagonalisation

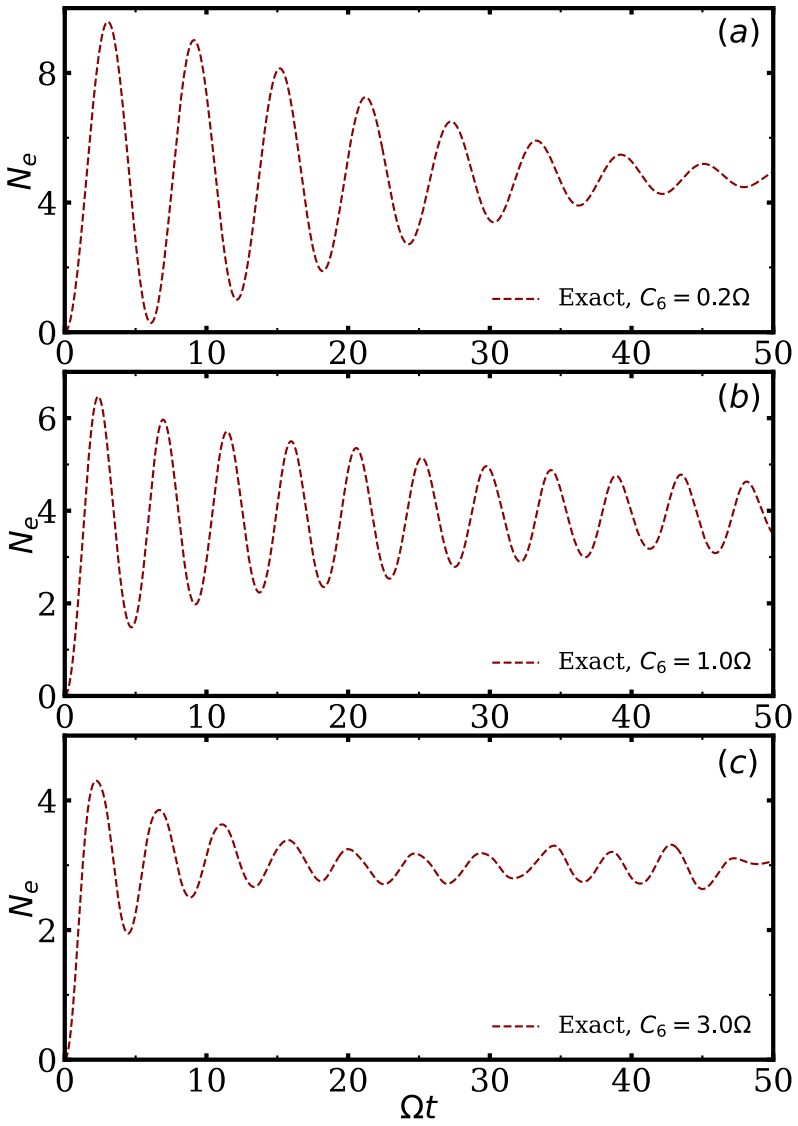

Figure 4.1: Excitation dynamics of an array of 10 atoms for different values of C_6 using Exact diagonalisation. In panel (a), we consider $C_6 = 0.2\Omega$. In panel (b), we consider $C_6 = 1\Omega$, and in panel (c), we take $C_6 = 3\Omega$.

Figure 4.1 shows the total number of excitations as a function of time for three different interaction strengths. We observe that the maximum number of excitations reduces as the interaction strength increases, and the oscillations also get smaller. This indicated the phenomena of the Rydberg

blockade discussed in chapter 2.

In figure 4.2, the plot of the maximum number of excitations as well as the average number of excitations as a function of interaction strength also clearly shows us the phenomenon of Rydberg blockade. We observe that the mean number of excitations has a kink near $C_6 = 1$, this is because, at that interaction strength, the blockade effects are felt at the nearest neighbour.

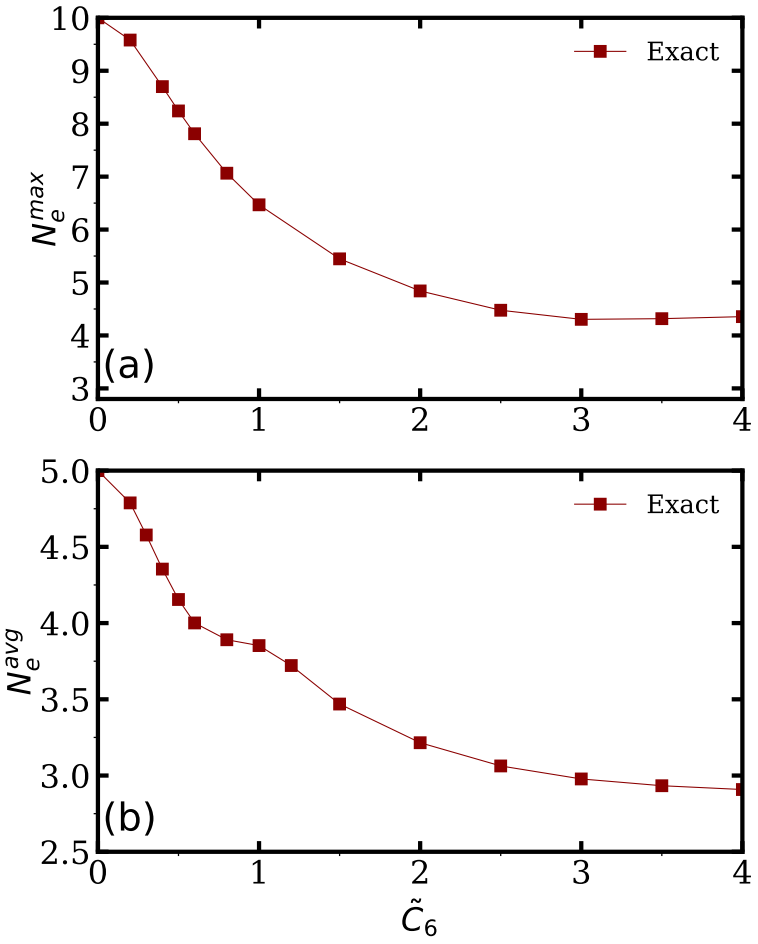

Figure 4.2: Maximum and the average number of total excitations as a function of interaction strengths (C_6) in an array of 10 atoms using Exact diagonalisation. In panel (a), we have the maximum number of excitations vs C_6. In panel (b), we have the average number of excitations vs C_6.

4.1.2 Results from dTWA

To get the excitation dynamics and time evolution using dTWA, we must first conduct a Monte Carlo sampling from the phase space of points.

Our initial state is $\rho_0 = \prod_i |g_i\rangle \langle g_i| = \prod_i |\downarrow_i\rangle \langle \downarrow_i|$, which when written in terms of Pauli matrices gives us

$$\rho_0 = \prod_i^N \left(\hat{I} - \sigma_i^z\right)/2 \tag{4.3}$$

From the expression for the phase point operator,

$$\hat{\mathscr{A}}_{\boldsymbol{\alpha}} = \frac{1}{2}\left[\hat{I} + \boldsymbol{r}_\alpha \cdot \boldsymbol{\sigma}\right] \tag{4.4}$$

We need to pick from the $\boldsymbol{r}_\alpha$ corresponding to our initial condition since, according to eqn. 3.41, the expectation value of the single spin operator is given by the average of a_i

$\boldsymbol{r}_\alpha$ is given by $\boldsymbol{r}_\alpha = ((-1)^{\alpha_2}, (-1)^{\alpha_1+\alpha_2}, (-1)^{\alpha_1})$, and we pick the initial conditions corresponding to $\boldsymbol{\alpha} = (1,0),(1,1)$ which gives us

$$\boldsymbol{r}_{(1,0)} = (1,-1,-1) \quad \boldsymbol{r}_{(1,1)} = (-1,1,-1)$$

Since the phase point operator is not uniquely defined, we can define the density matrix in the following manner

$$\hat{\rho}_0 = \sum_\alpha \mathscr{W}_\alpha \hat{A}_\alpha = \sum_\alpha \mathscr{W}_\alpha \frac{1}{2}\left(\hat{\mathscr{A}}_\alpha + \hat{\mathscr{A}}'_\alpha\right) \tag{4.5}$$

where $\hat{\mathscr{A}}'$ is defined using the following $\boldsymbol{r}$**'**

$$\boldsymbol{r}'_{(0,0)} = (1,-1,1), \quad \boldsymbol{r}'_{(0,1)} = (-1,1,1), \quad \boldsymbol{r}'_{(1,0)} = (1,1,-1), \quad \boldsymbol{r}'_{(1,1)} = (-1,1,-1) \tag{4.6}$$

and $\hat{A}_\alpha$ is given by

$$\tilde{\boldsymbol{r}}_{(0,0)} = (1,0,1), \quad \tilde{\boldsymbol{r}}_{(0,1)} = (-1,0,1), \quad \tilde{\boldsymbol{r}}_{(1,0)} = (1,0,-1), \quad \tilde{\boldsymbol{r}}_{(1,1)} = (-1,0,-1) \tag{4.7}$$

The above sampling scheme ignores fluctuations in the y-component of the three vectors. We can include them by including the following three vectors:

$$\tilde{\boldsymbol{r}}'_{(0,0)} = (0,1,1), \quad \tilde{\boldsymbol{r}}'_{(0,1)} = (0,-1,1), \quad \tilde{\boldsymbol{r}}'_{(1,0)} = (0,1,-1), \quad \tilde{\boldsymbol{r}}'_{(1,1)} = (0,-1,-1) \tag{4.8}$$

So, finally, we sample from $\tilde{r}_\alpha$ and $\tilde{r}'_\alpha$ and sample from

$$\{(1,0,-1),(-1,0,-1),(0,1,-1),(0,-1,-1)\}$$

Below, we present the results of the total number of excitations as a function of time using the 1st-order dTWA as well as the 2nd-order dTWA. The 2nd-order dTWA equations are numerically unstable, and this numerical instability is an inherent property of the differential equation, and the point of divergence does not depend on the size of the timestep.

In the equations of motion from eqn. 3.36, we were able to isolate the parts of the equation which are causing the divergence. We rewrite the equation for clarity.

$$\frac{1}{2}\dot{a}_i^\mu = \sum_\delta \left[\frac{\Omega}{2} a_i^\delta \in^{\mu x \delta} + \sum_i \sum_{j \neq i} \frac{V_{ij}}{4} a_i^\delta \in^{\mu z \delta} + \left(G_i^z a_i^\delta + G_i^{z\delta} \right) \in^{\mu z \delta} \right] \tag{4.9}$$

$$\begin{aligned}
\frac{1}{2}\dot{c}_{ij}^{\mu\nu} = &\sum_\beta \left[\left(\frac{V_{ij}}{4} a_i^\beta \ \delta_{\nu,z} - \frac{V_{ij}}{4} a_j^\beta \ \delta_{\mu,z} \right) \in^{\mu\nu\beta} \right] + \sum_\delta \left[\frac{\Omega}{2} c_{ij}^{\delta\nu} \in^{x\delta\mu} + \left(\sum_i \sum_{j \neq i} \frac{V_{ij}}{4} c_{ij}^{\delta\nu} + G_{i/}^z \, c_{ij}^{\delta\nu} \right) \in^{z\delta\mu} \right] \\
&+ \sum_\delta \left[\frac{\Omega}{2} c_{ij}^{\mu\delta} \in^{x\delta\nu} + \left(\sum_i \sum_{j \neq i} \frac{V_{ij}}{4} c_{ij}^{\mu\delta} + G_{j/}^z \, c_{ij}^{\mu\delta} \right) \in^{z\delta\nu} \right] + \sum_\delta \left[G_{ij}^{\nu z} a_i^\delta \ \in^{z\delta\mu} + G_{ji}^{\mu z} a_j^\delta \ \in^{z\delta\nu} \right] \\
&- \sum_\delta \frac{V_{ij}}{4} \left[a_i^\mu c_{ij}^{z\delta} \in^{z\delta\nu} + a_j^\nu c_{ij}^{\delta z} \ \in^{z\delta\mu} \right] - \sum_\delta \frac{V_{ij}}{4} \left[a_i^\mu \left(a_i^z a_j^\delta \right) \in^{z\delta\nu} + a_j^\nu \left(a_i^\delta a_j^z \right) \in^{z\delta\mu} \right]
\end{aligned} \tag{4.10}$$

where

$$G_i^z = \sum_{k\neq i} \frac{V_{ik}}{4} a_k^z \,, \qquad G_i^{z\delta} = \sum_{k\neq i} \frac{V_{ik}}{4} c_{ki}^{z\delta}$$
$$G_{ij}^z = \sum_{k\neq i,j} \frac{V_{ik}}{4} a_k^z \,, \qquad G_{ij}^{\nu z} = \sum_{k\neq i,j} \frac{V_{ik}}{4} c_{jk}^{\nu z}$$

If we split the equation of $c_{ij}^{\mu\nu}$ into 6 parts like

$$\frac{1}{2}\dot{c}_{ij}^{\mu\nu} = T_1 + T_2 + T_3 + T_4 + T_5 + T_6 \tag{4.11}$$

where

$$\begin{aligned}
T_1 &= \sum_{\beta} \left[\left(\frac{V_{ij}}{4} a_i^{\beta}\ \delta_{\nu,z} - \frac{V_{ij}}{4} a_j^{\beta}\ \delta_{\mu,z} \right) \in^{\mu\nu\beta} \right] \\
T_2 &= \sum_{\delta} \left[\frac{\Omega}{2} c_{ij}^{\delta\nu} \in^{x\delta\mu} + \left(\sum_i \sum_{j\neq i} \frac{V_{ij}}{4} c_{ij}^{\delta\nu} + G_{ij}^z\ c_{ij}^{\delta\nu} \right) \in^{z\delta\mu} \right] \\
T_3 &= \sum_{\delta} \left[\frac{\Omega}{2} c_{ij}^{\mu\delta} \in^{x\delta\nu} + \left(\sum_i \sum_{j\neq i} \frac{V_{ij}}{4} c_{ij}^{\mu\delta} + G_{ji}^z\ c_{ij}^{\mu\delta} \right) \in^{z\delta\nu} \right] \\
T_4 &= \sum_{\delta} \left[G_{ij}^{\nu z} a_i^{\delta} \in^{z\delta\mu} + G_{ji}^{\mu z} a_j^{\delta} \in^{z\delta\nu} \right] \\
T_5 &= -\sum_{\delta} \frac{V_{ij}}{4} \left[a_i^{\mu} c_{ij}^{z\delta} \in^{z\delta\nu} + a_j^{\nu} c_{ij}^{\delta z} \in^{z\delta\mu} \right] \\
T_6 &= -\sum_{\delta} \frac{V_{ij}}{4} \left[a_i^{\mu} \left(a_i^z a_j^{\delta} \right) \in^{z\delta\nu} + a_j^{\nu} \left(a_i^{\delta} a_j^z \right) \in^{z\delta\mu} \right]
\end{aligned} \tag{4.12}$$

We have observed that the main instability in the equation of motion for the 2-point correlation comes from T_4 and T_6, and by removing these terms from the equations of motion, for smaller interaction strengths, we were able to delay the time of divergence and also improve the results compared to 1st order dTWA, as is evident in figure (4.4). This becomes more difficult for stronger interactions, this is because the terms removed depend on the interaction strength, and these terms become more and more important at later times and larger interaction strengths.

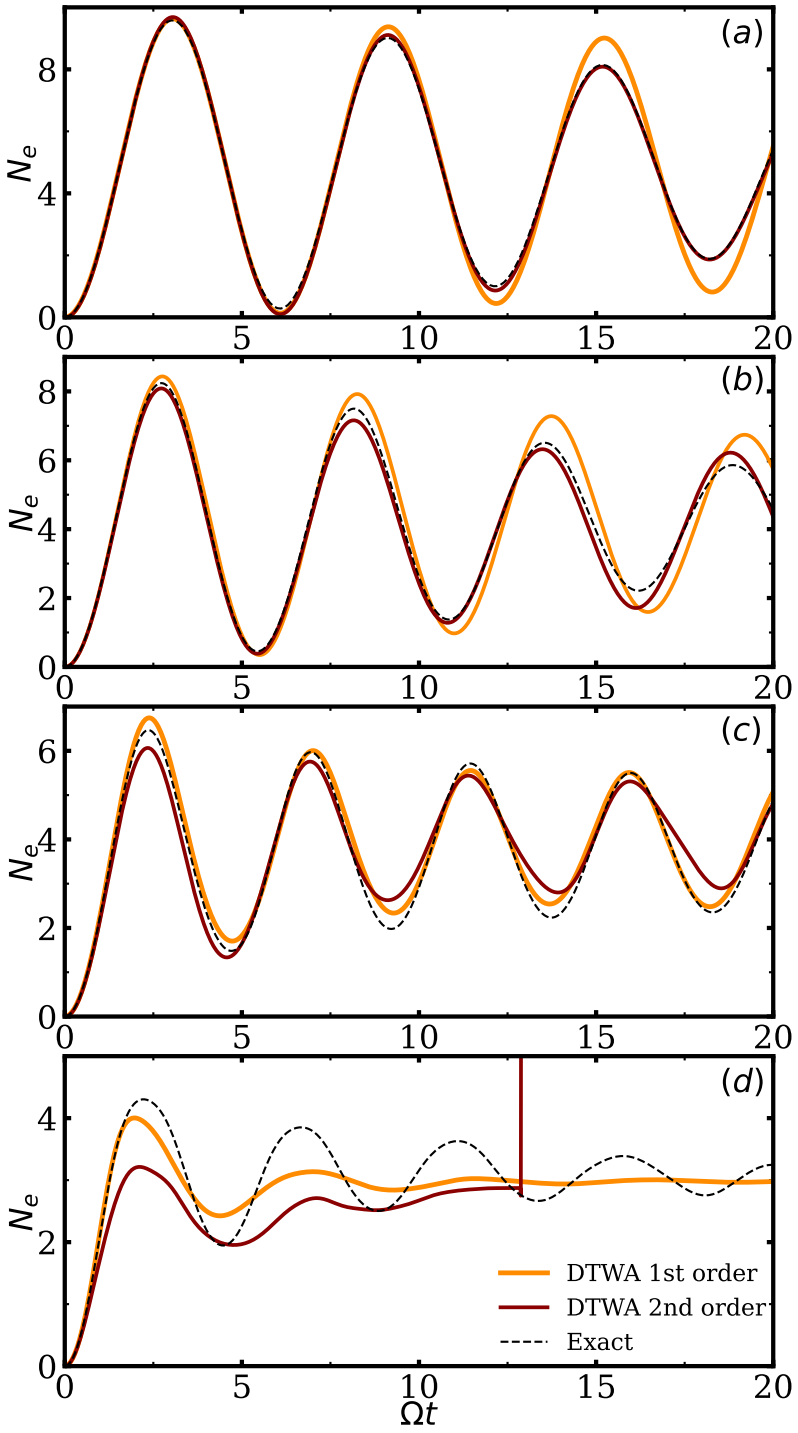

Figure 4.3: Excitation dynamics of an array of 10 atoms for different values of C_6 using 1st order and 2nd order dTWA and compared with exact results. In panel (a), we consider $C_6 = 0.2\Omega$. In panel (b), we consider $C_6 = 0.5\Omega$, in panel (c), we take $C_6 = 1\Omega$ and (d) we have $C_6 = 3\Omega$.

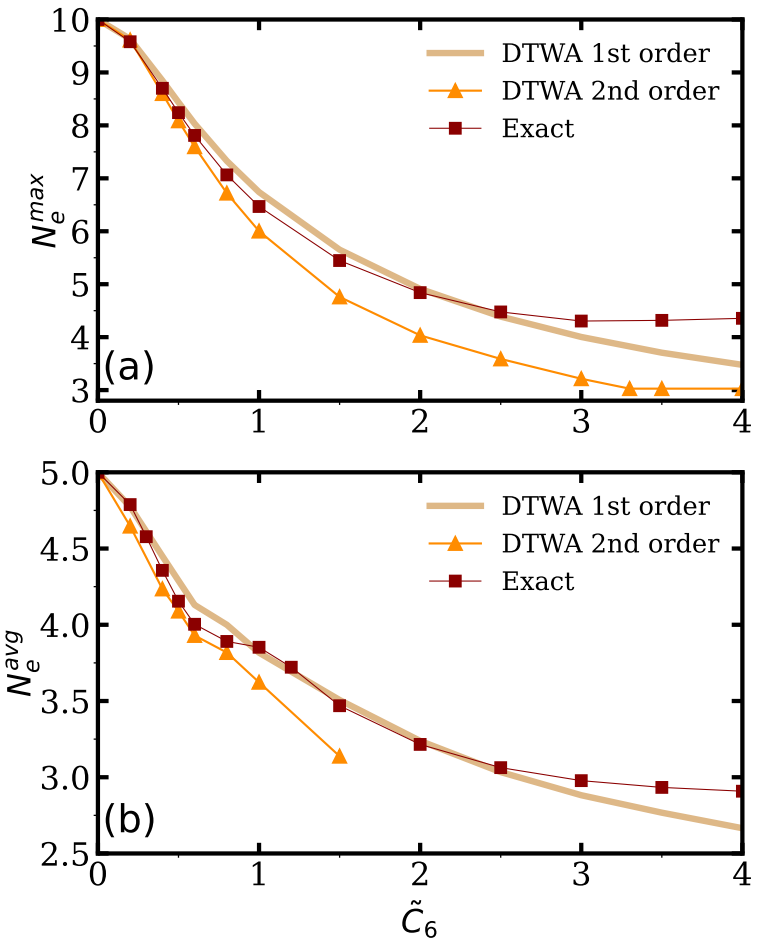

Figure 4.4: Maximum and the average number of total excitations as a function of interaction strengths (C_6) in an array of 10 atoms using 1st order dTWA and 2nd order dTWA compared with exact results. In panel (a), we have the maximum number of excitations vs C_6. In panel (b), we have the average number of excitations vs C_6.

We have also plotted the maximum number of excitations as well as the mean number of excitation using 1st and 2nd-order dTWA in figure 4.5. We can see that the 2nd-order dTWA is capturing the mean slightly better than the 1st-order dTWA at small interaction strengths.

4.1.3 Results from ANN

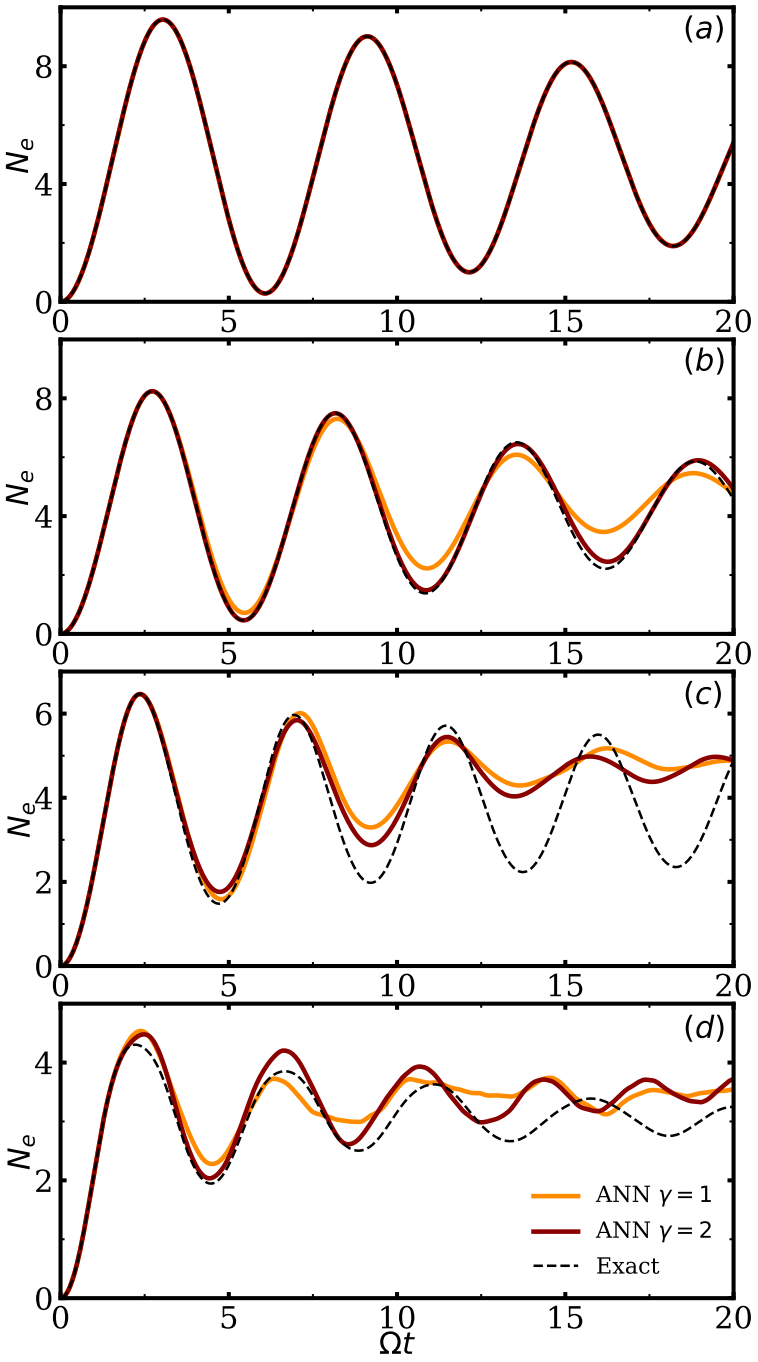

Figure 4.5: Excitation dynamics of an array of 10 atoms for different values of C_6 using ANN for a different number of hidden units and compared with exact results. In panel (a), we consider $C_6 = 0.2\Omega$. In panel (b), we consider $C_6 = 0.5\Omega$, in panel (c), we take $C_6 = 1\Omega$ and (d) we have $C_6 = 3\Omega$.

We look at the excitation dynamics of the 1D array of Rydberg atoms using neural networks, RBM in particular, with two different networks.

If N are the number of visible units in the input layer, which is equal to the number of spins considered, and M is the number of hidden units in the 2nd layer, we define γ as a quantitative measure of the size of our network, it is defined as the ratio of the number of hidden units to the number of visible units

$$\gamma = M/N$$

. Our initial condition is $\rho_0 = \prod_i |g_i\rangle \langle g_i| = \prod_i |\downarrow_i\rangle \langle \downarrow_i|$ But if we consider the system in the S_z basis, the covariance matrix S will be zero, and we cannot evolve the system. Hence we make a rotation around the Y axis where $S_z \to S_x$, $S_x \to -S_z$. Now in this S_x basis, we are able to choose an analytical initial condition where in the wavefunction using RBM,

$$\log(\Psi(S, \mathscr{W})) = \sum_{j=1}^{M} \log\cosh\left(b_j + \sum_{i=1}^{L} W_{ij} s_i\right) \tag{4.13}$$

We can choose the biases and weights to be zero, which then represents our initial condition.

In figure 4.5, we have the total number of excitations as a function of time for 2 different network sizes compared with the exact results. Like the universal approximation theorem says, we can approximate any complex function using an ANN provided we have a sufficient number of parameters, and so we can observe that on increasing the number of parameters by increasing the number of hidden units, the results have improved.

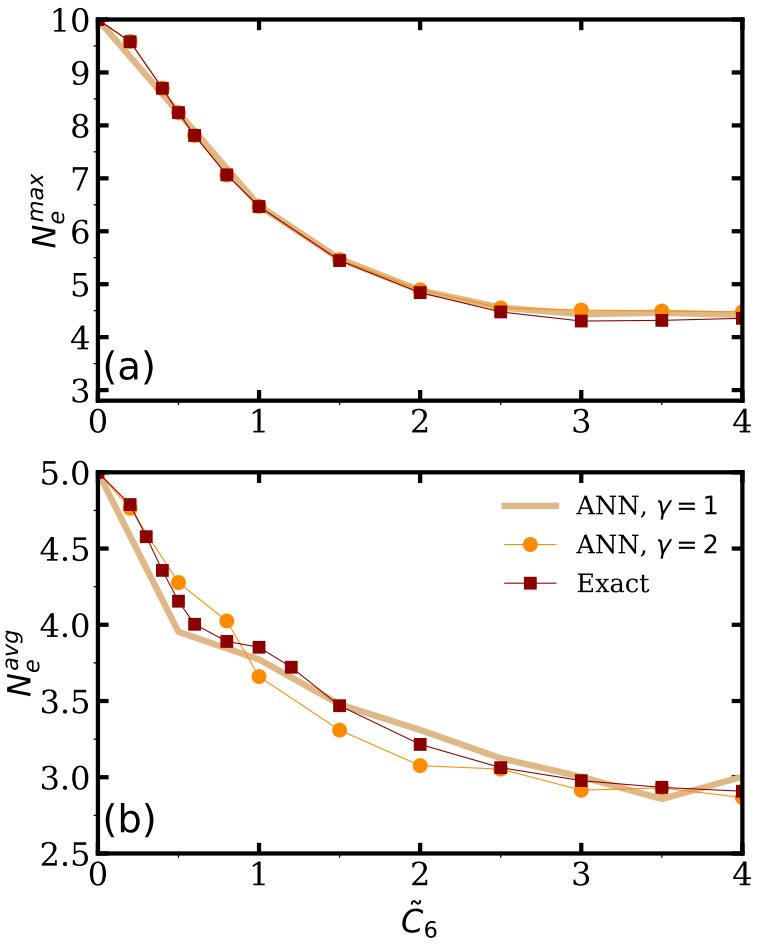

Figure 4.6: Maximum and the average number of total excitations as a function of interaction strengths (C_6) in an array of 10 atoms using ANN for 2 different hidden numbers of units compared with the exact results. In panel (a), we have the maximum number of excitations vs C_6. In panel (b), we have the average number of excitations vs C_6.

Comparison of excitation dynamics results with different ANN architectures

Here, we look at two different other networks. Both networks have the same number of hidden units as the visible units. In one network, we connect each visible unit to its corresponding unit and the nearest neighbours in the hidden layer. In the other network, we connect the visible unit with its corresponding unit in the hidden layer as well as its nearest neighbours and next-nearest neighbours in the hidden layer.

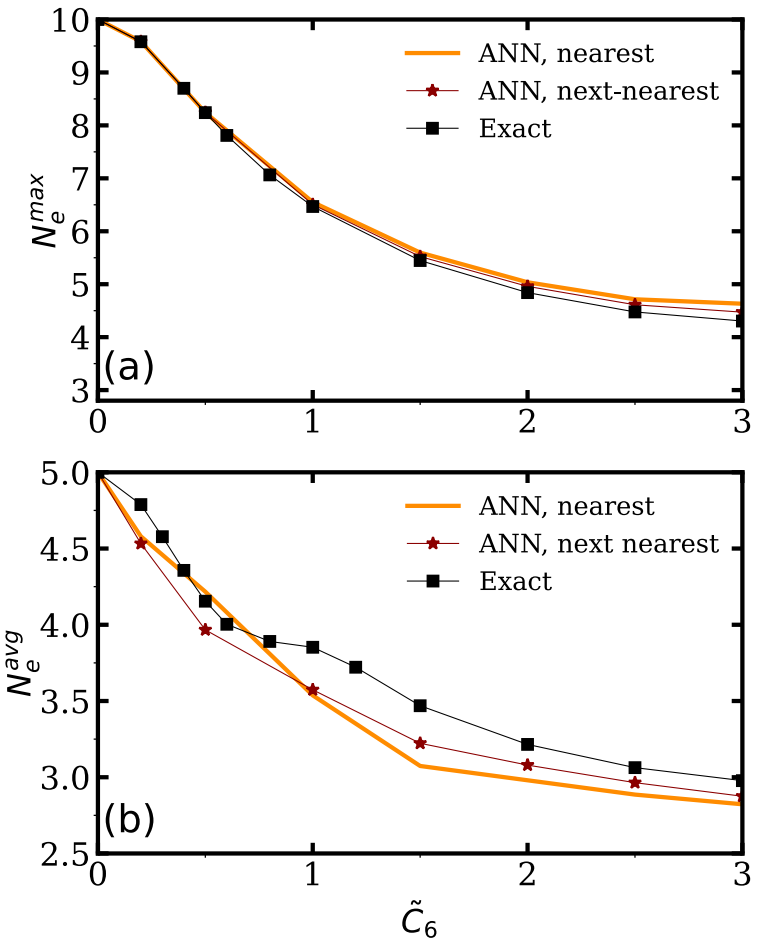

Figure 4.7: Maximum and the average number of total excitations as a function of interaction strengths (C_6) in an array of 10 atoms using ANN for 2 different architectures compared with the exact results. In panel (a), we have the maximum number of excitations vs C_6. In panel (b), we have the average number of excitations vs C_6.

In figure 4.7 (b), we see that for smaller interactions, the nearest neighbour network gives results that match better with the exact result, but for larger interactions beyond $C_6 = 1\Omega$, we see that the network incorporating the nearest neighbour as well as the next nearest neighbour connections matches better with the exact results. This is expected since as the interaction gets stronger, the next nearest neighbour connections start becoming important, and this kind of gives us an idea that even though the hidden units are not directly spins, they capture and learn the relation between the spins.

Energy while using ANN

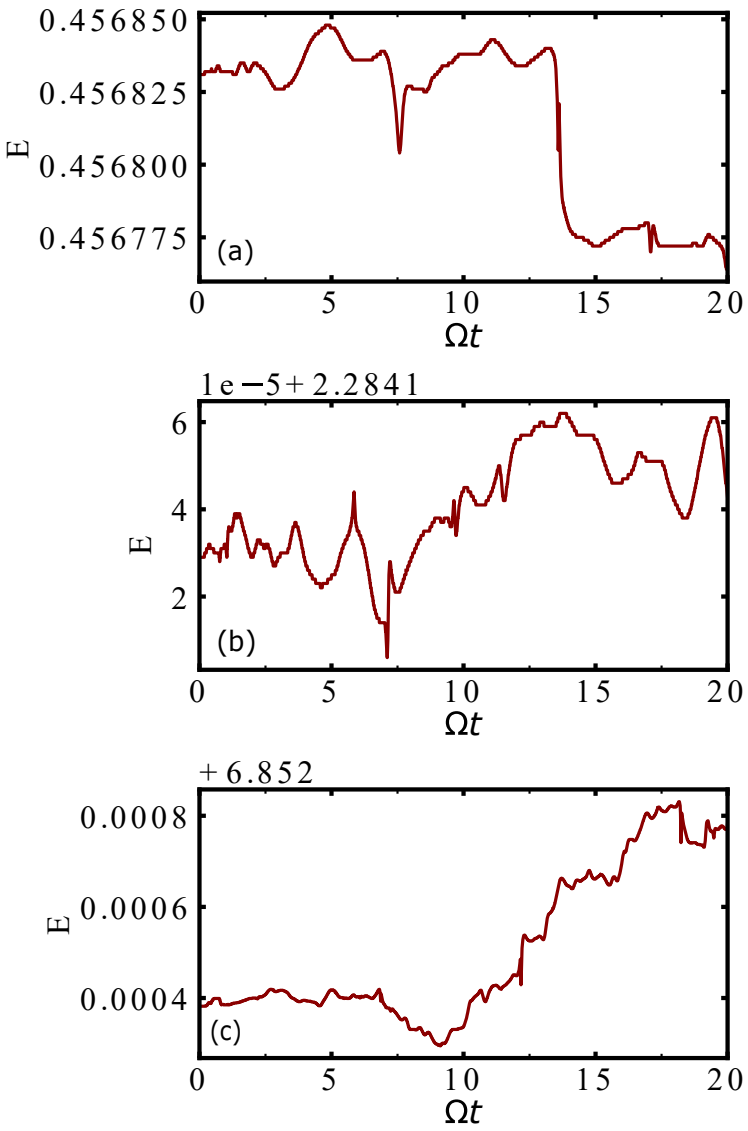

Figure 4.8: Expectation value of the energy during the unitary time evolution. In panel (a), we have $C_6 = 0.2\Omega$. In panel (b), we have $C_6 = 1\Omega$, and panel (c) has $C_6 = 3\Omega$.

In figure 4.8, we plot the expectation value of the energy as a function of time. We see that throughout the time evolution, the energy is constant up to the 4th decimal place, and the change is really small. This implies that the error in the dynamics is not a numerical error but due to the neural network not being completely able to represent the wave function.

4.2 Results of Entanglement Entropy dynamics

Entanglement is a valuable quantum resource for quantum information processing. It is one of the most important quantities to measure to verify that quantum simulators are performing as desired, as it provides signatures of a wide range of phenomena such as quantum criticality, topological phases, thermalization dynamics, and many-body localization. Moreover, large amounts of entanglement generation between different parts of the quantum system are necessary for quantum simulators and computers to provide an advantage over their classical counterparts. It can be quantified in many ways, such as the entanglement of creation, the entanglement of distillation and von Neumann entropy [69].

One important quantification of entanglement is entanglement entropy. Entanglement entropy has proven indispensable in the understanding of numerical methods and understanding how capable they are in describing quantum many-body states. A very interesting and important finding is the area law scaling of the entanglement entropy in 1D systems. This means that the scaling of the entropy is linear in the boundary area of the subsystem in question. One of the reasons the area law of entanglement entropy is important is because it gives an idea about how well or how easy it is for a numerical method is able to capture the properties of the quantum many-body system. In the case of DMRG, the scaling of entanglement specifies how well a given state can be approximated by a matrix-product state. And hence, in this thesis, we calculate the 2nd-order Rényi entanglement entropy using the numerical methods of dTWA and ANN.

Rényi α-entropy is a generalisation of the von Neumann entropy and reduces to the latter as α tends to 1. The Rényi α-entropy of a sub-system A is given by,

$$S(\alpha) = \frac{1}{N_A}\frac{1}{1-\alpha}\log(Tr([\hat{\rho}_A]^{\alpha})) \tag{4.14}$$

Where N_A is the number of particles in the subsystem and $\hat{\rho}_A$ is the reduced density matrix of subsystem A. When the entropy of subsystem A is greater than the entropy of the entire system $S_A(\alpha) > S(\alpha)$, there is bipartite entanglement between the subsystem and the rest of the system.

Below, we calculate the 2nd-order Rényi entanglement entropy using the numerical methods of dTWA and ANN.

4.2.1 dTWA approach to Rényi entropy

We calculate the Rényi entropy as done in [70]. Since the density operator can be expressed in terms of the Wigner function and the phase point operator, the Rényi entropy can also be expressed using the Wigner function. If the whole system is separated into subsystems A and B in real space, the 2nd-order Rényi entanglement entropy for subsystem A is given by

$$S_A^{(2)}(t) \equiv -\frac{1}{N_A}\log\left(Tr\{[\hat{\rho}_A(t)]^2\}\right) \tag{4.15}$$

where $\hat{\rho}_A(t)$ is the reduced density matrix of subsystem A and is given by the partial trace over B

$$\hat{\rho}_A(t) = Tr_B\hat{\rho}(t) \tag{4.16}$$

Using the phase point operator and the discrete Wigner function, the density matrix can be written as

$$\hat{\rho}(t) = \sum_\alpha W_\alpha(0)\hat{A}_\alpha(t) \tag{4.17}$$

In the first-order BBGKY hierarchy equation, we approximate the phase point operator as

$$\hat{A}_\alpha(t) = \prod_{i=1}^{M}\hat{A}_i(t,\alpha) \tag{4.18}$$

Then the reduced density matrix for A in terms of the Wigner function is

$$\begin{aligned}\hat{\rho}_A(t) &= Tr_B\left\{\sum_\alpha W_\alpha(0)\hat{A}_\alpha(t)\right\} \\ &= \sum_\alpha W_\alpha(0)\prod_{i\in A}\hat{A}_i(t,\alpha)\end{aligned} \tag{4.19}$$

To calculate the Rényi entropy we need to calculate $Tr\{[\hat{\rho}_A(t)]^2\}$,

$$\begin{aligned} Tr[\hat{\rho}_A(t)]^2 &= Tr\left(\sum_{\alpha,\alpha'} W_\alpha(0)W_{\alpha'}(0)\prod_{i\in A}\hat{A}_i(t,\alpha)\hat{A}_i(t,\alpha')\right) \\ &= \sum_{\alpha,\alpha'} W_\alpha(0)W_{\alpha'}(0)Tr\left[\prod_{i\in A}\frac{1}{4}(\mathscr{I}+\sum_\mu a_i^\mu(t)\hat{\sigma}_\mu^i)(\mathscr{I}+\sum_\mu a_i'^\mu(t)\hat{\sigma}_\mu^i)\right] \\ &= \sum_{\alpha,\alpha'} W_\alpha(0)W_{\alpha'}(0)\prod_{i\in A}\frac{1}{2}\left[\mathscr{I}+\sum_\mu a_i^\mu(t)a_i'^\mu(t)\right] \end{aligned} \tag{4.20}$$

Using 4.15 and 4.20 we can write the the 2nd-order Rényi entropy as

$$S_A^{(2)}(t) = -\frac{1}{N_A}\log\left[\sum_{\alpha,\alpha'} W_\alpha(0)W_{\alpha'}(0)\prod_{i\in A}\frac{1}{2}\left(\mathscr{I}+\sum_\mu a_i^\mu(t)a_i'^\mu(t)\right)\right] \tag{4.21}$$

where $a_i(0) = \mathbf{r}_{\alpha_i}$ and $a_i'(0) = \mathbf{r}_{\alpha_i'}$.

Here, $a_i(t)$ and $a_i'(t)$ are the classical spins evolved using the 1st order equation in the BBGKY hierarchy. The initial conditions, $\mathbf{r}_{\alpha_i}$ and $\mathbf{r}_{\alpha_i'}$ are sampled using sampling IV, and these two separate trajectories are evolved independently and the ensemble average of $\prod_{i\in A}\frac{1}{2}\left(\mathscr{I}+\sum_\mu a_i^\mu(t)a_i'^\mu(t)\right)$ is taken to then calculate the Rényi entropy using 4.21

The Monte Carlo sampling causes a constant shift in the value of the Rényi entropy, which we correct for by dividing by $Tr\{[\hat{\rho}_A(0)]^2\}$

To calculate the 2nd order Rényi entanglement entropy using ANN, we use 4.15 where we get the reduced density matrix ρ_A from the neural quantum states using QuTiP [71] [72]

4.2.2 Results for Half-chain 2nd-order Rényi entanglement entropy

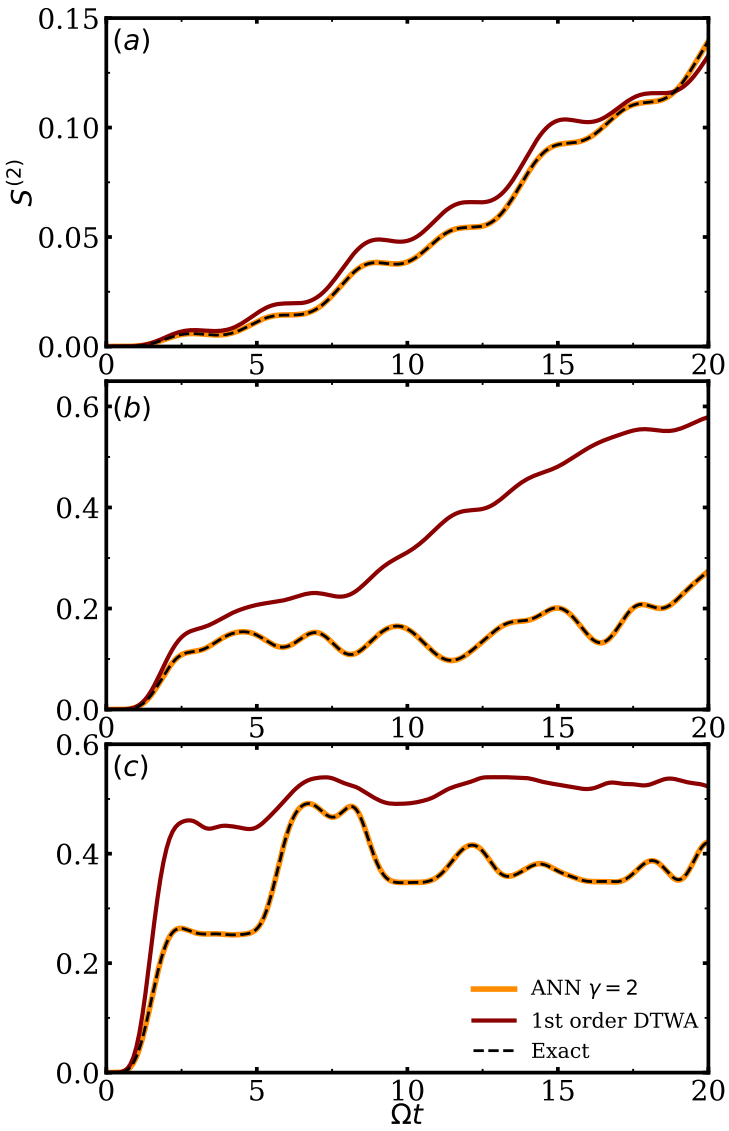

Figure 4.9: Half-chain Rényi entanglement entropy as a function of Ωt using ANN and dTWA and compared with the exact dynamics for 4 atoms for different values of C_6. In panel (a), we consider $C_6 = 0.2\Omega$ and in panel (b), we consider $C_6 = 1\Omega$ and in panel (c), we take $C_6 = 3\Omega$.

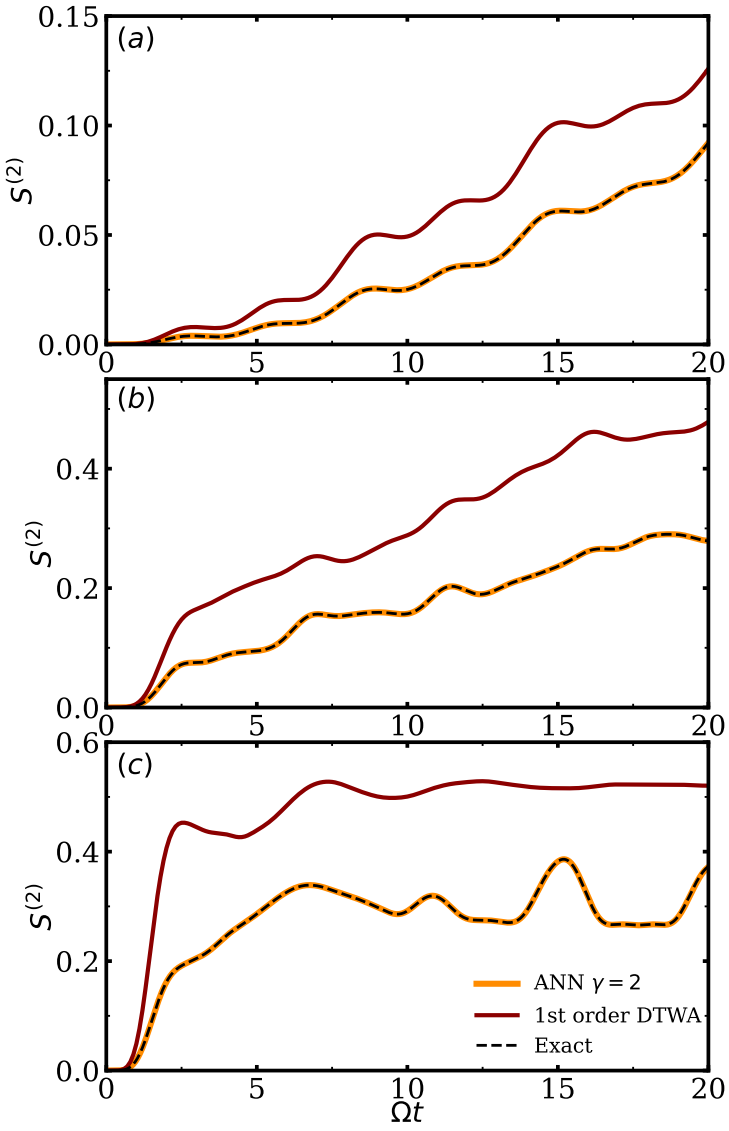

Figure 4.10: Half-chain Rényi entanglement entropy as a function of Ωt using ANN and dTWA and compared with the exact dynamics for 6 atoms for different values of C_6. In panel (a), we consider $C_6 = 0.2\Omega$ and in panel (b), we consider $C_6 = 1\Omega$ and in panel (c), we take $C_6 = 3\Omega$.

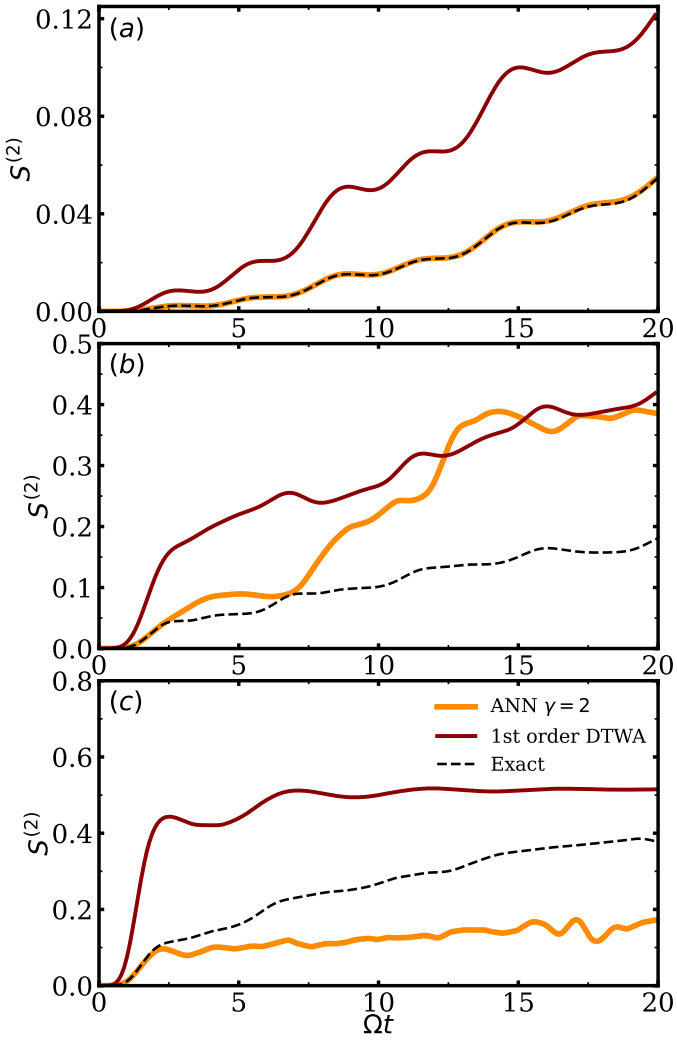

Figure 4.11: Half-chain Rényi entanglement entropy as a function of Ωt using ANN and dTWA and compared with the exact dynamics for 10 atoms for different values of C_6. In panel (a), we consider $C_6 = 0.2\Omega$ and in panel (b), we consider $C_6 = 1\Omega$ and in panel (c), we take $C_6 = 3\Omega$.

We see that ANN is able to capture the entanglement growth very well, and it matches perfectly with the exact results for smaller system sizes of $N = 4$ and $N = 6$ but does not do so well in case of $N = 10$. In the case of dTWA, since it is an approximation and the expression for the density matrix in 4.16 it is not able to capture the growth in entanglement exactly, but we can observe that it is able to capture the qualitative features of the entanglement entropy and the features like the bumps very well for small interaction strengths.

Comparison of half-chain Rényi entanglement entropy with different ANN architectures

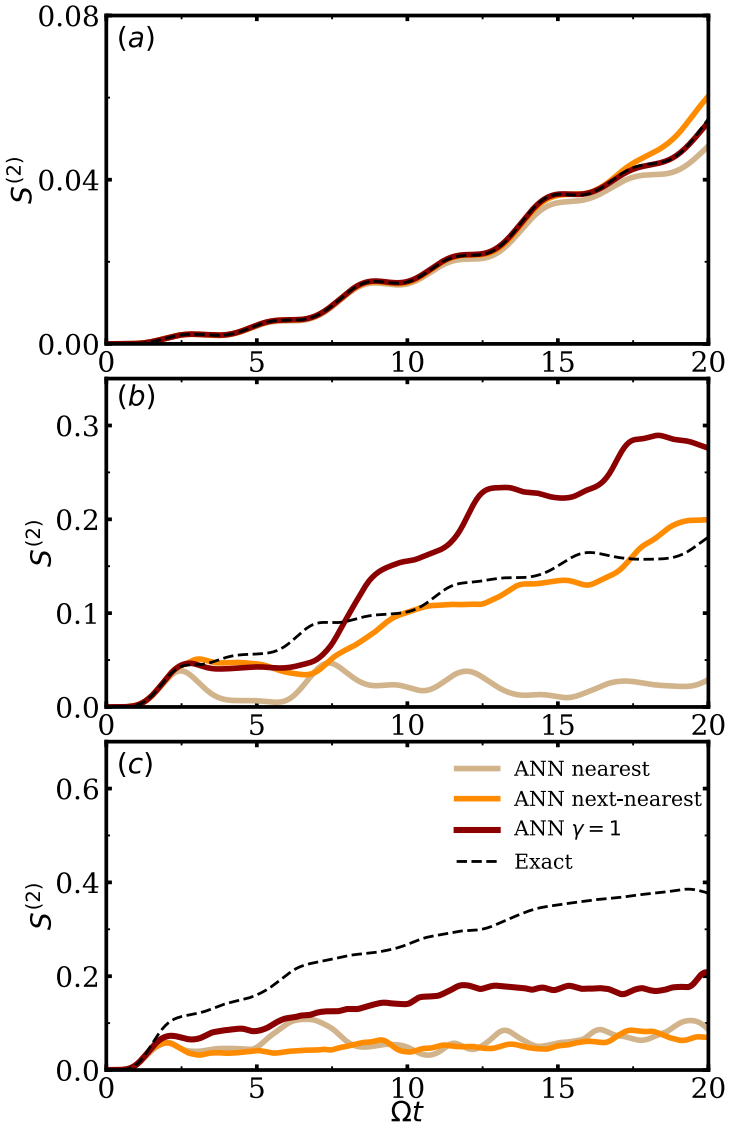

Figure 4.12: Half-chain Rényi entanglement entropy as a function of Ωt using ANN for two different networks for different values of C_6 for 10 atoms. In panel (a), we consider $C_6 = 0.2\Omega$ and in panel (b), we consider $C_6 = 1\Omega$ and in panel (c), we take $C_6 = 3\Omega$.

In figure 4.12, we consider two different networks similar to 4.7 where we consider the same number of visible and hidden units, and in one network, we link the unit in the visible unit with the corresponding unit in the hidden layer along with the neighbouring units in the hidden layer.

In the other network, we link the unit in the visible unit with the corresponding unit in the hidden layer along with the neighbours and next-nearest neighbours in the hidden layer. We see that for $C_6 = 0.2\Omega$, all the networks capture the entropy pretty well. For $C_6 = 1\Omega$, the nearest neighbour network works the best, and for higher still, interaction strength of $C_6 = 3\Omega$, all to all connections of the RBM work the best. So essentially, increasing the connections to the nearest and nearest neighbour interactions works better as we increase the interaction strength.

A note on the purity in dTWA

In dTWA, we construct the density matrix using the phase point operator and the discrete Wigner function given by $\rho(t) = \sum_\alpha \mathscr{W}_\alpha \hat{\mathscr{A}}_\alpha$. The purity of the density matrix gives us a quantitative measure of whether the state is pure or mixed and is given by

$$P(t) = \mathrm{Tr}[\rho^2] \tag{4.22}$$

If $|i\rangle$ are the orthogonal basis states, a pure state is given by $|\psi\rangle = \sum_i c_i |i\rangle$ and the density matrix of this state is given by $\rho_p = |\psi\rangle \langle\psi|$. A mixed state given by $\rho_m = \sum_i |\psi_i\rangle \langle\psi_i|$ is a statistical mixture of pure states and cannot be written as the out product of any single state.

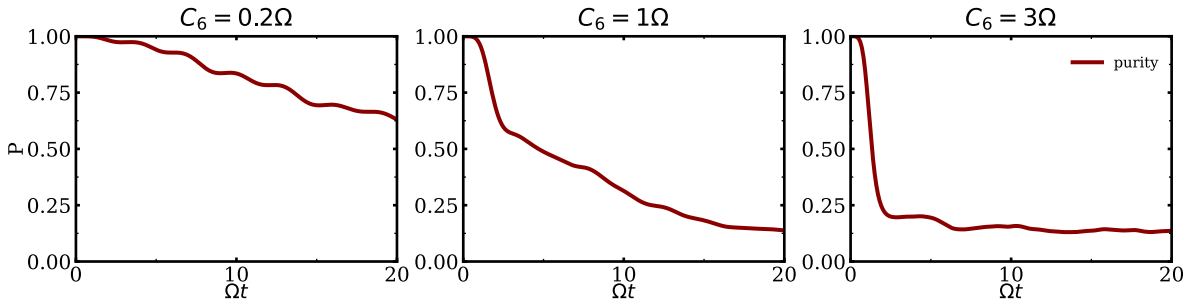

Figure 4.13: Purity of the density matrix as a function of Ωt using dTWA for different values of C_6 for 4 atoms. In panel (a), we consider $C_6 = 0.2\Omega$ and in panel (b), we consider $C_6 = 1\Omega$ and in panel (c), we take $C_6 = 3\Omega$.

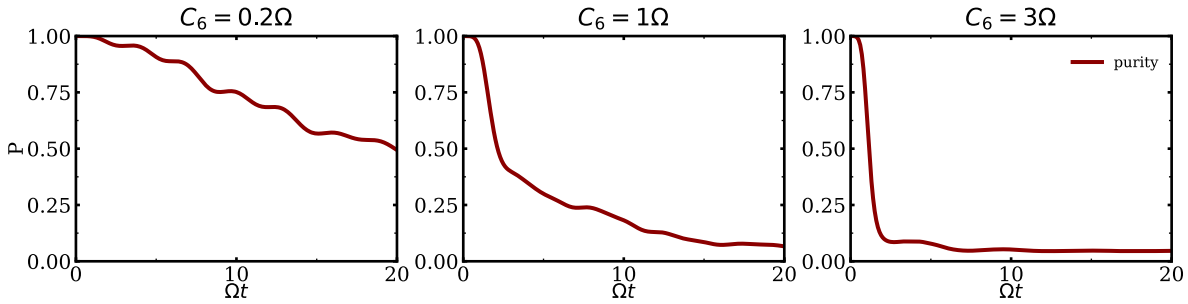

Figure 4.14: Purity of the density matrix as a function of Ωt using dTWA for different values of C_6 for 6 atoms. In panel (a), we consider $C_6 = 0.2\Omega$ and in panel (b), we consider $C_6 = 1\Omega$ and in panel (c), we take $C_6 = 3\Omega$.

In figure 4.13 and 4.14, we have plotted the purity as a function of time for $N = 4$ and $N = 6$ using the 1st order dTWA. We see that the purity is not maintained as a function of time since our density matrix is an approximation since we assume that the phase point operator is the tensor product of the individual phase point operator of each atom $\hat{\mathscr{A}}_{\boldsymbol{\alpha}_1} \otimes \hat{\mathscr{A}}_{\boldsymbol{\alpha}_2} \otimes ..... \otimes \hat{\mathscr{A}}_{\boldsymbol{\alpha}_N}$ and hence, the purity deteriorates and is not maintained. We also see that the purity deteriorates more as we increase the interaction strength, this is probably because as the interaction increases, the correlation increases and the approximation that the phase point operator is the tensor product does not hold. We also observe that even though the purity deteriorates, dTWA is able to capture the excitation dynamics pretty well.

Chapter 5

Conclusion

In conclusion, we have studied the excitation and correlation dynamics of a chain of Rydberg atoms having van de Waal type of interaction using the numerical methods of discrete truncated Wigner approximation and artificial neural networks. We have looked at the total number of excitations as a function of time, along with the maximum number of excitations reached at any point and the mean number of excitations. We have also looked at the growth of the half-chain entanglement entropy.

We have observed that in the case of dTWA, the 1st-order dTWA is able to capture the excitation dynamics fairly well for intermediate timescales and smaller interaction strengths. On including the correlations and using the 2nd-order dTWA, we have observed that the equations are inherently numerically unstable, as is also observed by others. We have tried to rectify this issue by figuring out the terms in the equation of motion of the 2-point correlations that were causing this instability and have eliminated them to observe that even though the divergence still occurs, for small interaction strengths, we are able to delay the divergence significantly and also provide an improvement from the 1st order dTWA. We have also looked at the 2nd-order Renyi entanglement entropy using 1st-order dTWA, and we observe that due to the dTWA being an approximation, it captures the growth of entanglement entropy only for a small system and for small interaction

strengths. We have also looked at the purity of the density matrix, and on account of dTWA being an approximation, the purity of the state is not maintained, yet it is able to capture the dynamics pretty well.

In the case of Artificial neural networks, we have observed that it is able to capture the excitation dynamics for the total number of excitations as well as the average number of excitations well, we see an improvement in the results as we increase the number of parameters used. We have also calculated the 2nd-order renyi entanglement entropy using ANN. We observe that for system size $N = 4$ and $N = 6$, ANN captures the entanglement growth perfectly. But, for $N = 10$, we see that for larger interaction strengths, it is not able to capture the entanglement entropy that well. We also looked at two other networks and looked at the regimes in which those networks work better. We plot the expectation value of the energy and see that during the unitary time evolution, the energy remains fairly constant.

In conclusion, with the fast-paced developments in Rydberg quantum simulators, theoretical and numerical tools to study and benchmark with the Rydberg quantum simulators are needed to be developed. In this thesis, we look at the numerical methods of discrete truncated Wigner approximation and Artificial neural networks and apply them to a one-dimensional chain of Rydberg atoms with van der Waal interactions. We have tested the range of validity of the numerical methods, and in the case of the numerically unstable 2nd-order dTWA, we have identified the terms causing the divergences and delayed the diverges and improved the results in the case of small interactions.

Further work can be done in exploring other neural network architectures to study this system and also in including higher order dTWA and see if this solves the instability in the equation of motion of the 2-point correlation.

Bibliography

[1] Tomoyuki Yamakami. Computational complexity measures of multipartite quantum entanglement. In *International Symposium on Algorithms and Computation*, 2003.

[2] Richard Phillips Feynman. Simulating physics with computers. *International Journal of Theoretical Physics*, 21:467–488, 1999.

[3] Juan Ignacio Cirac and Peter Zoller. Goals and opportunities in quantum simulation. *Nature Physics*, 8:264 – 266, 2012.

[4] Hendrik Weimer, Markus Michael Muller, Igor Lesanovsky, Peter Zoller, and Hans Peter Buchler. A rydberg quantum simulator. *Nature Physics*, 6:382–388, 2009.

[5] Antoine Browaeys and Thierry Lahaye. Many-body physics with individually controlled rydberg atoms. *Nature Physics*, 16:132 – 142, 2020.

[6] Hannes Bernien, Sylvain Schwartz, A. Keesling, H. Levine, Ahmed Omran, Hannes Pichler, Soonwon Choi, A. S. Zibrov, Manuel Endres, Markus Greiner, Vladan Vuletić, and Mikhail D. Lukin. Probing many-body dynamics on a 51-atom quantum simulator. *Nature*, 551:579–584, 2017.

[7] Malte Schlosser, Daniel Ohl de Mello, Dominik Schäffner, Tilman Preuschoff, Lars Kohfahl, and Gerhard Birkl. Assembled arrays of rydberg-interacting atoms. *Journal of Physics B: Atomic, Molecular and Optical Physics*, 53, 2020.

[8] Hyosub Kim, Yeje Park, Kyungtae Kim, H. S. Sim, and Jaewook Ahn. Detailed balance of thermalization dynamics in rydberg-atom quantum simulators. *Physical review letters*, 120 18:180502, 2017.

[9] Elmer Guardado-Sanchez, Peter T. Brown, Debayan Mitra, Trithep Devakul, David A. Huse, Peter Schauss, and Waseem S. Bakr. Probing the quench dynamics of antiferromagnetic correlations in a 2d quantum ising spin system. *Physical Review X*, 2018.

[10] S Ebadi, Tout T. Wang, H. Levine, A. Keesling, G. Semeghini, Ahmed Omran, D. Bluvstein, Rhine Samajdar, Hannes Pichler, Wen Wei Ho, Soonwon Choi, Subir Sachdev, Markus Greiner, Vladan Vuletić, and Mikhail D. Lukin. Quantum phases of matter on a 256-atom programmable quantum simulator. *Nature*, 595:227 – 232, 2020.

[11] D. Bluvstein, Ahmed Omran, H. Levine, A. Keesling, G. Semeghini, S Ebadi, T. T. Wang, A A Michailidis, Nishad Maskara, Wen Wei Ho, S. Choi, Maksym Serbyn, Markus Greiner, Vladan Vuletić, and Mikhail D. Lukin. Controlling quantum many-body dynamics in driven rydberg atom arrays. *Science*, 371:1355 – 1359, 2021.

[12] R. Islam, C. Senko, W. C. Campbell, S. Korenblit, J. Smith, A. Lee, E. E. Edwards, C.-C. J. Wang, J. K. Freericks, and C. Monroe. Emergence and frustration of magnetism with variable-range interactions in a quantum simulator. *Science*, 340(6132):583–587, 2013.

[13] Nicolai Friis, Oliver Marty, Christine Maier, Cornelius Hempel, Milan Holzäpfel, Petar Jurcevic, Martin B. Plenio, Marcus Huber, Christian Roos, Rainer Blatt, and Ben Lanyon. Observation of entangled states of a fully controlled 20-qubit system. *Phys. Rev. X*, 8:021012, Apr 2018.

[14] Colin D. Bruzewicz, John Chiaverini, Robert McConnell, and Jeremy M. Sage. Trapped-ion quantum computing: Progress and challenges. *Applied Physics Reviews*, 6(2):021314, 2019.

[15] John L. Bohn, Ana Maria Rey, and Jun Ye. Cold molecules: Progress in quantum engineering of chemistry and quantum matter. *Science*, 357(6355):1002–1010, 2017.

[16] A. Patscheider, B. Zhu, L. Chomaz, D. Petter, S. Baier, A.-M. Rey, F. Ferlaino, and M. J. Mark. Controlling dipolar exchange interactions in a dense three-dimensional array of large-spin fermions. *Phys. Rev. Research*, 2:023050, Apr 2020.

[17] A. de Paz, A. Sharma, A. Chotia, E. Maréchal, J. H. Huckans, P. Pedri, L. Santos, O. Gorceix, L. Vernac, and B. Laburthe-Tolra. Nonequilibrium quantum magnetism in a dipolar lattice gas. *Phys. Rev. Lett.*, 111:185305, Oct 2013.

[18] Román Orús. A practical introduction to tensor networks: Matrix product states and projected entangled pair states. *Annals of Physics*, 349:117–158, 2013.

[19] White. Density matrix formulation for quantum renormalization groups. *Physical review letters*, 69 19:2863–2866, 1992.

[20] Ulrich Schollwoeck. The density-matrix renormalization group in the age of matrix product states. *Annals of Physics*, 326:96–192, 2010.

[21] Guifré Vidal. Efficient simulation of one-dimensional quantum many-body systems. *Phys. Rev. Lett.*, 93:040502, Jul 2004.

[22] Steven R. White and Adrian E. Feiguin. Real-time evolution using the density matrix renormalization group. *Phys. Rev. Lett.*, 93:076401, Aug 2004.

[23] A J Daley, C Kollath, U Schollwöck, and G Vidal. Time-dependent density-matrix renormalization-group using adaptive effective hilbert spaces. *Journal of Statistical Mechanics: Theory and Experiment*, 2004(04):P04005, apr 2004.

[24] Steven R. White and Adrian E. Feiguin. Real-time evolution using the density matrix renormalization group. *Physical review letters*, 93 7:076401, 2004.

[25] Anatoli Polkovnikov. Phase space representation of quantum dynamics. *Annals of Physics*, 325:1790–1852, 2009.

[26] J. Schachenmayer, A. Pikovski, and A. M. Rey. Many-body quantum spin dynamics with monte carlo trajectories on a discrete phase space. *Phys. Rev. X*, 5:011022, Feb 2015.

[27] Reyhaneh Khasseh, Angelo Russomanno, Markus Schmitt, Markus Heyl, and Rosario Fazio. Discrete truncated wigner approach to dynamical phase transitions in ising models after a quantum quench. *Phys. Rev. B*, 102:014303, Jul 2020.

[28] Stefanie Czischek, Martin Gärttner, Markus Oberthaler, Michael Kastner, and Thomas Gasenzer. Quenches near criticality of the quantum ising chain power and limitations of the discrete truncated wigner approximation. *Quantum Science and Technology*, 4(1):014006, oct 2018.

[29] Michael A. Perlin, Chunlei Qu, and Ana Maria Rey. Spin squeezing with short-range spin-exchange interactions. *Phys. Rev. Lett.*, 125:223401, Nov 2020.

[30] Bihui Zhu, Ana Maria Rey, and Johannes Schachenmayer. A generalized phase space approach for solving quantum spin dynamics. *New Journal of Physics*, 21(8):082001, aug 2019.

[31] Mehrtash Babadi, Eugene A. Demler, and Michael Jason Knap. Far-from-equilibrium field theory of many-body quantum spin systems: Prethermalization and relaxation of spin spiral states in three dimensions. *arXiv: Quantum Gases*, 2015.

[32] Asier Piñeiro Orioli, Arghavan Safavi-Naini, Michael L. Wall, and Ana Maria Rey. Nonequilibrium dynamics of spin-boson models from phase space methods. *Physical Review A*, 96:033607, 2017.

[33] Asier Piñeiro Orioli, Adrien Signoles, H Wildhagen, G. Günter, J urgen Berges, Shannon Whitlock, and Matthias Weidemüller. Relaxation of an isolated dipolar-interacting rydberg quantum spin system. *Physical review letters*, 120 6:063601, 2017.

[34] Jacob P. Covey, Luigi De Marco, Oscar L. Acevedo, Ana Maria Rey, and Jun Ye. An approach to spin-resolved molecular gas microscopy. *New Journal of Physics*, 20, 2018.

[35] Oscar L. Acevedo, Arghavan Safavi-Naini, Johannes Schachenmayer, Michael L. Wall, Rahul M. Nandkishore, and Ana Maria Rey. Exploring many-body localization and thermalization using semiclassical methods. *Physical Review A*, 96:033604, 2017.

[36] Giuseppe Carleo and Matthias Troyer. Solving the quantum many-body problem with artificial neural networks. *Science*, 355(6325):602–606, 2017.

[37] G. Fabiani and J. H. Mentink. Investigating ultrafast quantum magnetism with machine learning. *SciPost Phys.*, 7:4, 2019.

[38] Markus Schmitt and Markus Heyl. Quantum many-body dynamics in two dimensions with artificial neural networks. *Phys. Rev. Lett.*, 125:100503, Sep 2020.

[39] Stefanie Czischek, Martin Gärttner, and Thomas Gasenzer. Quenches near ising quantum criticality as a challenge for artificial neural networks. *Phys. Rev. B*, 98:024311, Jul 2018.

[40] Yukai Wu, L.-M. Duan, and Dong-Ling Deng. Artificial neural network based computation for out-of-time-ordered correlators. *Phys. Rev. B*, 101:214308, Jun 2020.

[41] Moritz Reh, Markus Schmitt, and Martin Gärttner. Time-dependent variational principle for open quantum systems with artificial neural networks, 2021.

[42] Michael J. Hartmann and Giuseppe Carleo. Neural-network approach to dissipative quantum many-body dynamics. *Phys. Rev. Lett.*, 122:250502, Jun 2019.

[43] Di Luo, Zhuo Chen, Juan Carrasquilla, and Bryan K. Clark. Autoregressive neural network for simulating open quantum systems via a probabilistic formulation, 2021.

[44] Florian Schäfer, Takeshi Fukuhara, Seiji Sugawa, Yosuke Takasu, and Yoshiro Takahashi. Tools for quantum simulation with ultracold atoms in optical lattices. *Nature Reviews Physics*, pages 1–15, 2020.

[45] Christian Gross and Immanuel Bloch. Quantum simulations with ultracold atoms in optical lattices. *Science*, 357:1001 – 995, 2017.

[46] Florence Nogrette, Henning Labuhn, Sylvain Ravets, Daniel Barredo, Lucas B'eguin, Aline Vernier, Thierry Lahaye, and Antoine Browaeys. Single-atom trapping in holographic 2d arrays of microtraps with arbitrary geometries. *Physical Review X*, 4:021034, 2014.

[47] Woojun Lee, Hyosub Kim, and Jaewook Ahn. Three-dimensional rearrangement of single atoms using actively controlled optical microtraps. *Optics express*, 24 9:9816–25, 2016.

[48] Daniel Barredo, Vincent Lienhard, Sylvain de Léséleuc, Thierry Lahaye, and Antoine Browaeys. Synthetic three-dimensional atomic structures assembled atom by atom. *Nature*, 561:79–82, 2017.

[49] T F Gallagher. Rydberg atoms. *Reports on Progress in Physics*, 51:143 – 188, 1988.

[50] Felix Engel, Thomas Dieterle, Thomas Schmid, Christian Tomschitz, Christian Veit, N. Zuber, Robert Löw, Tilman Pfau, and Florian Meinert. Observation of rydberg blockade induced by a single ion. *Physical review letters*, 121 19:193401, 2018.

[51] Hannes Pichler, Sheng-Tao Wang, Leo Zhou, Soonwon Choi, and Mikhail D. Lukin. Computational complexity of the rydberg blockade in two dimensions. *ArXiv*, abs/1809.04954, 2018.

[52] Jaksch, Cirac, Zoller, Rolston, Côté, and Lukin. Fast quantum gates for neutral atoms. *Physical review letters*, 85 10:2208–11, 2000.

[53] Mikhail D. Lukin, Michael Fleischhauer, Robin Côté, Luming Duan, Dieter Jaksch, Juan Ignacio Cirac, and Peter Zoller. Dipole blockade and quantum information processing in mesoscopic atomic ensembles. *Physical review letters*, 87 3:037901, 2000.

[54] Xiaoling Wu , Xinhui Liang , Yaoqi Tian , Fan Yang , Cheng Chen , Yong Liu , Meng Khoon Tey , and Lixing You . A concise review of rydberg atom based quantum computation and quantum simulation. *Chinese Physics B*, 30, 2021.

[55] J. Smith, A. C. Lee, P. Richerme, Brian Neyenhuis, Paul W Hess, Philipp Hauke, Markus Heyl, David A. Huse, and Christopher Monroe. Many-body localization in a quantum simulator with programmable random disorder. *Nature Physics*, 12:907 – 911, 2015.

[56] Jonathan Simon, Waseem S. Bakr, Ruichao Ma, M. Eric Tai, Philipp M. Preiss, and Markus Greiner. Quantum simulation of antiferromagnetic spin chains in an optical lattice. *Nature*, 472:307–312, 2011.

[57] R. Islam, Crystal Senko, W. C. Campbell, Simcha Korenblit, J. Smith, A. C. Lee, Emily E. Edwards, C.C.-Joseph Wang, James K. Freericks, and Christopher R. Monroe. Emergence and frustration of magnetism with variable-range interactions in a quantum simulator. *Science*, 340:583 – 587, 2012.

[58] A. Keesling, Ahmed Omran, H. Levine, Hannes Bernien, Hannes Pichler, Soonwon Choi, Rhine Samajdar, Sylvain Schwartz, Pietro Silvi, Subir Sachdev, Peter Zoller, Manuel Endres, Markus Greiner, Vladan Vuletić, and Mikhail D. Lukin. Quantum kibble–zurek mechanism and critical dynamics on a programmable rydberg simulator. *Nature*, 568:207–211, 2018.

[59] J. H. Zhang, Guido Pagano, Paul W Hess, A. Kyprianidis, Pascal Becker, Harvey B. Kaplan, Alexey V. Gorshkov, Zhe-Xuan Gong, and Christopher R. Monroe. Observation of a many-body dynamical phase transition with a 53-qubit quantum simulator. *Nature*, 551:601–604, 2017.

[60] Vighnesh Naik, Varna Shenoy, Weibin Li, and Rejish Nath. Analyzing rydberg excitation dynamics in an atomic chain via discrete truncated wigner approximation and artificial neural networks. 2021.

[61] E. Wigner. On the quantum correction for thermodynamic equilibrium. *Phys. Rev.*, 40:749–759, Jun 1932.

[62] William B. Case. Wigner functions and weyl transforms for pedestrians. *American Journal of Physics*, 76:937–946, 2008.

[63] Anatoli Polkovnikov. Phase space representation of quantum dynamics. *Annals of Physics*, 325(8):1790–1852, 2010.

[64] Lorenzo Pucci, Analabha Roy, and Michael Kastner. Simulation of quantum spin dynamics by phase space sampling of bogoliubov-born-green-kirkwood-yvon trajectories. *Phys. Rev. B*, 93:174302, May 2016.

[65] William K Wootters. A wigner-function formulation of finite-state quantum mechanics. *Annals of Physics*, 176(1):1–21, 1987.

[66] William K. Wootters. The discrete wigner function a. *Annals of the New York Academy of Sciences*, 480, 1986.

[67] Michael Bonitz. *The Method of Reduced Density Operators*, pages 313–340. Springer, Cham, Dordrecht, 2016.

[68] Han-Qing Shi, Xiao-Yue Sun, and Ding-Fang Zeng. Neural-network quantum state of transverse-field ising model. *Communications in Theoretical Physics*, 71(11):1379, nov 2019.

[69] Yu-Xin Wang, Liang-Zhu Mu, Vlatko Vedral, and Heng Fan. Entanglement rényi α entropy. *Phys. Rev. A*, 93:022324, Feb 2016.

[70] Masaya Kunimi, Kazuma Nagao, Shimpei Goto, and Ippei Danshita. Performance evaluation of the discrete truncated wigner approximation for quench dynamics of quantum spin systems with long-range interactions. *Phys. Rev. Res.*, 3:013060, Jan 2021.

[71] J.R. Johansson, P.D. Nation, and Franco Nori. Qutip 2: A python framework for the dynamics of open quantum systems. *Computer Physics Communications*, 184(4):1234–1240, 2013.

[72] J.R. Johansson, P.D. Nation, and Franco Nori. Qutip: An open-source python framework for the dynamics of open quantum systems. *Computer Physics Communications*, 183(8):1760–1772, 2012.